View Article Online
View Journal

Journal of Materials Chemistry A

Materials for energy and sustainability

Accepted Manuscript

This article can be cited before page numbers have been issued, to do this please use: M. Xu, C. Lai, X. Liu, B. Li, M. Zhang, F. Xu, S. Liu, L. Li, L. Qin, H. Yi, Y. Fu, L. Yang and Y. Li, *J. Mater. Chem. A*, 2021, DOI: 10.1039/D1TA04439G.

ROYAL SOCIETY OF CHEMISTRY

rsc.li/materials-a

View Article Online
DOI: 10.1039/D1TA04439G

COFs-confined catalysts: From nanoparticle and nanocluster to single atoms

Mengyi Xu [a, b] Cui Lai [a, b, *], Xigui Liu [a, b, †], Bisheng Li [a, b], Mingming Zhang [a, b], Fuhang Xu [a, b], Shiyu Liu [a, b], Ling Li [a, b], Lei Qin [a, b], Huan Yi [a, b], Yukui Fu [a, b]

[a] College of Environmental Science and Engineering, Hunan University, Changsha 410082, Hunan, PR China

[b] Key Laboratory of Environmental Biology and Pollution Control (Hunan University), Ministry of Education, Changsha 410082, Hunan, PR China

* Corresponding author at: College of Environmental Science and Engineering, Hunan University, Changsha, Hunan 410082, China. Tel.: +86–731– 88822754; fax: +86–731–88823701. E-mail address: laicui@hnu.edu.cn (C. Lai)

† Corresponding author at: College of Environmental Science and Engineering, Hunan University, Changsha, Hunan 410082, China. Tel.: +86–731– 88822754; fax: +86–731–88823701. E-mail address : liuxigui@hnu.edu.cn (X. G. Liu)

View Article Online
DOI: 10.1039/D1TA04439G

Abstract: In the heterogeneous catalytic reaction, nano-scale particles (nanoparticle, nanocluster, and single atoms) display excellent performance due to their different electronic structures, particle sizes, and geometric shapes. However, nano-scale particles are easy to aggregate and inactivate, confining nano-scale particles in crystalline porous materials is a best way to solve the above problems. Covalent organic framework with high crystallinity, high porosity, and tunable structure will be a potential alternative, which has attracted substantial attention. More importantly, the interaction between nano-scale particles and supports (confinement effect) could be controlled through the different synthetic methods. The confinement effect has great significance to the performance of the catalysts, for example, size effect for activity promotion, encapsulation effect for stability enhancement, and molecular-sieving effect for selectivity improvement. Therefore, the confinement effect of COFs-confined catalysts provides the functional sites for catalytic reactions. There has been a major breakthrough in solving the problems of environmental pollution and energy shortage. The efficiency of heterogeneous catalytic reactions such as hydrogen production, carbon dioxide reduction reaction, 4-nitrophenol reduction, hydrogenation reaction, and organic pollutant degradation have been improved by using COFs-confined catalysts. Herein, the synthetic methods of nano-scale particles confined in COFs are summarized, and the interaction between nano-scale particles and COFs are discussed to understand their various confinement effects. Then, the interaction between nano-scale particles and the reactant was understood through heterogeneous catalytic reactions. Finally, perspectives on the future developments about COFs-confined catalysts in various

View Article Online
DOI: 10.1039/D1TA04439G

fields are highlighted.

Key words: COFs-confined catalysts; Nanoparticles; Nanoclusters; Single atoms; Heterogeneous catalytic reaction

View Article Online
DOI: 10.1039/D1TA04439G

1. Introduction

Heterogeneous catalysis is the change in activity from one surface to the next.[1] This kind of surface catalysis science mostly occurs in solid catalysts and is mostly used in industrial environmental purification and energy storage reactions.[2] The heterogeneous catalytic system composed of nano-scale particles (from nanoparticle and nanocluster to single atoms) usually display excellent catalytic performance due to their high ratio of surface area to volume. However, the nano-scale particles are easy to agglomerate and deactivate, thereby reducing their catalytic performance.[3, 4] In order to obtain heterogeneous catalytic system with high catalytic activity, Kobosev et al. studied the catalytic behavior of supported catalysts from the viewpoint of atomic dispersion,[5] which laid a foundation for the development of porous materials as carrier materials for nano-scale particles dispersion. Many porous supports, such as carbon materials,[6] metal oxide,[7] zeolites,[8] graphene,[9] porous organic polymers (POPs),[10] and metal organic frameworks (MOFs)[11] have been reported. These materials have been used for confining nano-scale particles through size control, facet adjustment, and morphology modulation. The interaction between nano-scale particles and porous support is strong, which can prevent the nano-scale particles from aggregation.[12] However, due to the low stability and uneven pore distribution of these materials, they are still not ideal alternatives for stabilizing ultrafine nano-scale particles.[13] Wherefore, the development of porous material that can synthesize uniform nano-scale particles to improve the availability of materials is still the focus of heterogeneous catalysts.

Covalent organic frameworks (COFs) is a new porous and ordered crystalline

View Article Online
DOI: 10.1039/D1TA04439G

polymer connected by light elements (C, H, O, N) through covalent bonds.[14-17] Compared with reported others materials, it has the characteristics of high crystallinity, high porosity, coordinated topological structure, and convenient functional design.[18-23] Benefiting from these unique advantages, COFs have attracted much attention in the field of heterogeneous catalysis, covering a lot of fields such as gas storage and separation, photocatalysis, electrocatalysis, and photo-electrocatalysis.[23-25] In these studies, the excellent properties of COF-embedded nanoparticles for heterogeneous catalysis were mentioned intermittently, providing a new vision for future research of COF.[26, 27] Meanwhile, COF is also a potential alternative to confine nano-scale particles owing to following superiorities: (1) The covalent bond between the blocks ensures the physical and chemical stability of nano-sized particles in the COFs;[10] (2) The pore size different COF building blocks can be adjusted to accommodate different nanoscale particles;[17] (3) The unique channel structure of COFs provide efficient access to active sites;[28] (4) The permanent mesoporous structure of COFs can well restrict the nano-scale particles and prevent them from agglomeration and deactivation;[22] (5) The conjugated system of COFs facilitates the transport of electrons and optimizes the catalytic performance.[29] The superiorities of COFs reflect in the catalytic activity, stability, and selectivity in heterogeneous catalysis.

As we all know, the interaction between nano-scale particles (from nanoparticle and nanocluster to single atoms) and COFs supports is closely relevant to supports types, particle types, support pore size.[30-32] Compared with traditional supported catalysts in which metal nanoparticles are supported on solid oxides, the nano-scale particles

View Article Online
DOI: 10.1039/D1TA04439G

supported on COFs-confined catalysts enrich the structure-reaction relationship (such as structure control, size control, position design etc.).[2, 4, 33] The activity of these COFs-confined catalysts depends on the restriction effects (such as synergistic effect, constraint characteristics, target recognition performance) between the nano-scale particles and the supports framework, which will change the electronic structure and catalytic activity of the particles.[13, 34, 35] This restriction effect provides researchers with a reasonable design plan, allowing them to more precisely control the structure and stability of the active site.[2, 36]

Thus, in this review, we discuss the incorporation of nano-scale particles into crystalline microporous COFs and COF-based materials. We also detailly summarize the important heterogeneous catalytic applications and structure-reactivity correlations of nano-scale particles confined in COFs or COF-based materials. We start from introducing the strategy of isolating nano-scale particles in COFs, and then the influence of different synthesis strategies on the size of nano-particles and the configuration of the support is described. And the superiority of COFs as a support and the different catalytic activities produced by confinement effects are further explained through different heterogeneous catalytic reactions. Finally, the practical application of COFs-confined catalysts is discussed, and the future development is also prospected.

2. Design and synthesis of catalysts

For the metal nanoparticles confined in the porous organic framework, the interaction between metal nanoparticles and porous skeleton exists at the interface (Fig.1a), and this metal-support interaction can limit the particle growth to a specific

View Article Online
DOI: 10.1039/D1TA04439G

size to reduce particle aggregation.[37] Therefore, the COF-based materials with nanochannels can be designed and synthesized by precisely controlling the structure of heteroatoms, and nanochannels facilitate the entry of nano-scale particles so that the size and shape of nano-scale particles (from nanoparticle, nanocluster, and single atoms) can be reasonably controlled in the nanochannel.[38] This controllable strategy of nano-sized particles breaks the limitation of the pore size of carrier and realizes the controllable synthesis of ultra-fine nanoparticles and large-size nanoparticles (Fig.1a). Hence, according to the formation pathway of nano-scale particles, the synthetic methods of COFs-confined catalysts are mainly divided into following categories (Fig.1b): (1) nano-scale particles were in-suit synthesized in the pores of COF through the formation of particle ligand precursors; (2) The smaller structural units interact with each other to self-assembly and non-self-assembly form COFs-confined catalysts; (3) Selecting the appropriate construction unit to form COFs or COF-based material, and then form COFs-confined catalysts through the post-modification strategy.

View Article Online
DOI: 10.1039/D1TA04439G

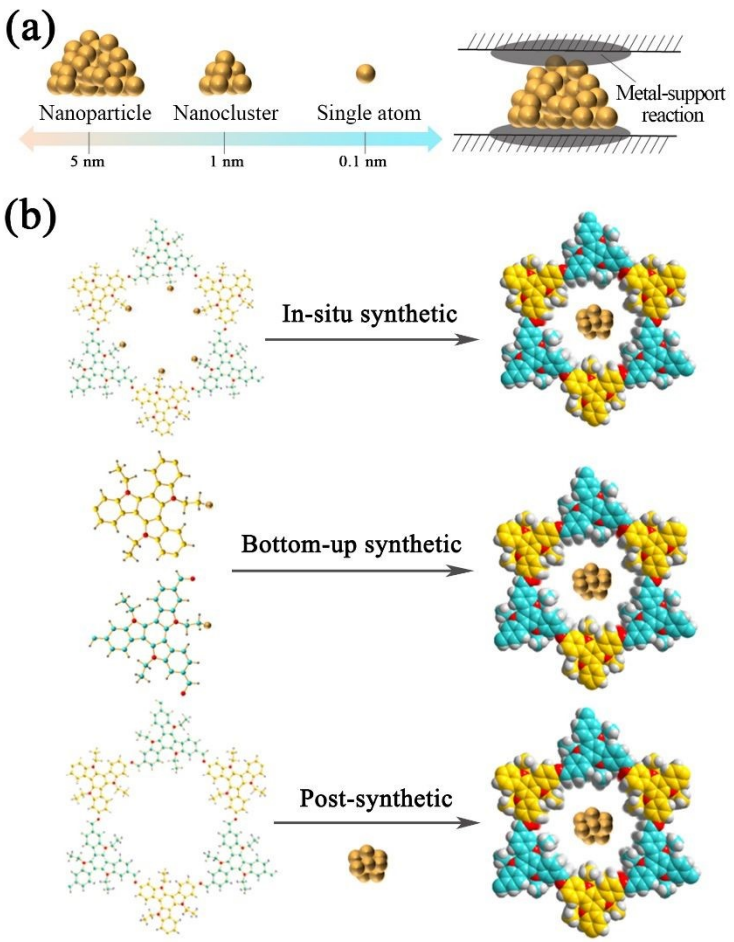

Fig. 1 (a) For nano-scale particles (nanoparticle, nanocluster, and single atom) and metal clusters supported on conventional, open-structure solid carriers; (b) The illustration of the synthesis routes and representative images of different COFs-confined catalysts.

2.1 In-situ synthetic method

Metal ions can be pre-embedded into the pores of COFs or COF-based materials through special functional groups or bonding with COF constituent units, and then metal ions can be reduced to nano-scale particles in-situ by some conventional reducing agents (such as $NaBH_4$).[39] This in-situ synthetic method can maintain the original crystal porous structure of COFs and control the growth of particles. Although there are few reports on the in-situ synthesis of COFs-confined materials, the formation of

View Article Online
DOI: 10.1039/D1TA04439G

precursors of the pre-synthesized materials by ion replacement and the in-situ reduction of ions into ultrafine nano-scale particles in COFs has attracted wide attention.[40, 41] Because the former two methods need to add reducing agents and other reagents to assist the synthesis of materials, it not only increases the cost but also introduces new impurities. Therefore, some researchers have prepared nano-scale particles without using external reducing agents by carbon-carbon and carbon-heteroatom bonding reactions (Fig. 2a).[42] It not only reduces the experimental steps but also reduces the damage of the external reducing agent to the crystal structure. Although these in-situ synthetic methods can synthesize COFs-confined materials, the nano-scale particles of size cannot be precisely controlled in the COF pores by in-suit methods, which may lead to pore blockage or non-uniformity of the formed nano-scale particles, thereby resulting in the failure of material synthesis.

Allowing nano-scale particles to nucleate and grow spontaneously in the pores of COFs or COF-based materials in a fixed form can save tedious pretreatment processes. During the synthetic process, the formation of bond bridges (Au-S-COF) by in-suit generating gold nanoclusters (Au NCs) in the optimized COFs pores is considered to be the most ideal means to simplify the synthetic process.[43] Compared with other examples, Au NCs are more prone to aggregation, leading poor loading to effect and reducing catalytic activity. [44] However, the formed Au-S-COF bridge can well inhibit aggregation and improve the catalytic activity. By selecting the appropriate building block to adjust the structure of COF, the active center can be introduced quickly and conveniently. However, the formed bond bridge is uncertain. In order to develop more

View Article Online
DOI: 10.1039/D1TA04439G

accurate and concise in-situ synthetic methods, some researchers have found that when designed and synthesized a well-defined COFs containing triazine groups (CTFs), the replacement or modification of the pyridine nitrogen heteroatom has no effect on the structure of CTFs, thereby we can effectively synthesis ultrafine Pt or Pd nanoparticles through optimizing the pyridine nitrogen heteroatom.[45] In terms of the crystal growth and particle size of catalyst, the close interrelationship between pyridine nitrogen and metal leads to the ultrafine synthesize of nanoparticles. The success of the in-situ synthesis of COFs-confined materials depends on the design of the precursors of COFs or COF-based materials, such as the design of pore size, the choice of anchored nano-scale particles, and the selection of COF building blocks.

2.2 Bottom-up synthetic method

There are many synthetic methods for synthesizing heterogeneous catalysts, and the most used methods are bottom-up synthetic methods, including sol-gel method, co-precipitation method, solution impregnation method, wet-chemistry impregnation dispersion method, and other chemical methods.[46, 47] However, the conventional bottom-up synthetic methods cannot satisfy the formation of COFs-confined materials. In the case of CTFs as the substrate, the use of impregnation combined with solvothermal method to deposit cadmium sulfide nanoparticles (CdS NPs) is compared with impregnation combined with photo-deposition approach of CdS NPs. The nanoparticles formed by the photo-deposition approach are smaller, and it can expose more active sites.[48] This method solves the randomness and looseness of CdS NPs loading on the support, and precisely controls the loading position of nano-scale

View Article Online
DOI: 10.1039/D1TA04439G

162 particles. Although the bottom-up synthetic method can accurately control the
163 morphology and structure of the material, it is difficult to synthesize a material dense
164 surface load.[22] But, the calcination method can be used to reduce Fe^{3+} on the surface of
165 COFs to prepare the single-atom Fe embedded in the COFs and reduce loading amount
166 (Fig. 2b).[49] This process requires strict control in the ratios of Fe precursor/COFs, to
167 realize strong durability and catalytic activity. In addition, the wet-chemistry immersion
168 dispersion method used to load Pd NPs into the optimized COFs (COF-SO_3H), which
169 also can achieve low loading content.[50] In the synthetic process, the loading of Pd will
170 not change the structure of the catalyst, and a low-content loading is achieved, thereby
171 supplying more easily available active sites.

172 In some cases, COFs with free active functional groups synthesized by a bottom-
173 up method can be used to anchor nano-scale particles well.[51] Nitrogen atoms in COFs
174 with nitrogen donor function can stabilize metal NPs and control the growth of metal
175 NPs.[52] For example, the CTFs synthesized by the bottom-up method are used to anchor
176 Ru NPs well.[53] Compared with other synthetic methods, it has the advantages of high
177 catalytic stability and strong recyclability. Moreover, the internal structure of COFs
178 also can be changed by adding triazine groups to supply an effective channel for loading
179 metal nanoparticles.[54] The triazine group and COFs can form a two-dimensional (2D)
180 hexagonal system through one-pot polycondensation method, which makes it easier to
181 infuse silver nanoparticles into the pores of COFs, thereby improving the synthesis
182 efficiency. In a bottom-up synthetic strategy, we can synthesize COFs-confined
183 catalysts with good stability and compatibility by modifying COF monomers.

View Article Online
DOI: 10.1039/D1TA04439G

2.3 Post-synthetic modification method

The introduction of nano-scale particles into COFs or COFs-based materials by post-synthetic modification is the most common method to obtain COFs-confined materials.[55] For instance, the bipyridine groups are embedded in COFs by post-synthetic modification method. This method not only provides binding sites for non-noble metal atoms, but also improves the electron transfer inside COFs molecules.[56] As a new type of crystalline material, COFs have a large specific surface area and high content of heteroatoms (non-carbon atom), and excellent gas capture performance,[38, 57] but their charge separation ability needs to be improved. However, the post-synthesis modification method can be used to precisely adjust the electronic properties and energy band structure, and to strengthen the interaction between the nano-scale particles and the COFs support, resulting in improved catalytic activity of the heterogeneous catalytic system.[58] For some special materials, the corresponding functional catalyst can be obtained by double post-treatment. For example, Zhang et al. introduced gold NPs into propylene functionalization COF (P-COF) through a post-modification strategy, and gold NPs with a narrow particle size distribution were successfully loaded on P-COF (Fig. 2c).[59] The modification of COFs through these grafting or chemical reactions makes it of great significance for us to achieve controllable structure and excellent performance for COFs-confined catalysts.

Due to the tunability of COFs, the aperture size of COFs can be adjusted arbitrarily by selecting suitable blocks to meet actual needs.[60] Therefore, the modified nanoparticles can be loaded into the COFs through post-modification strategies. Two

View Article Online
DOI: 10.1039/D1TA04439G

teams are currently exploring this strategy to synthesize COFs-confined heterogeneous catalysts.[61, 62] In these works, different encapsulation materials (polyvinylpyrrolidone (PVP) and zeolitic imidazolate framework-8 (ZIF-8)) are first used to treat the nanoparticles to avoiding agglomeration and deactivation. Compared with the stronger bond and function in COFs to control the growth of nanoparticles, this strategy can better control the size and morphology of nanoparticles, thereby accurately controlling the catalytic activity of catalyst. Besides, R. Vaidhyanathan et al. proposed to load nanoparticles in COF channels using double solvent method (have yielded metallic Ni_3N nanoparticles of the size < 5 nm),[63] which could provide a new idea for precise control of the size of nanoparticles in COFs-confined catalysts.

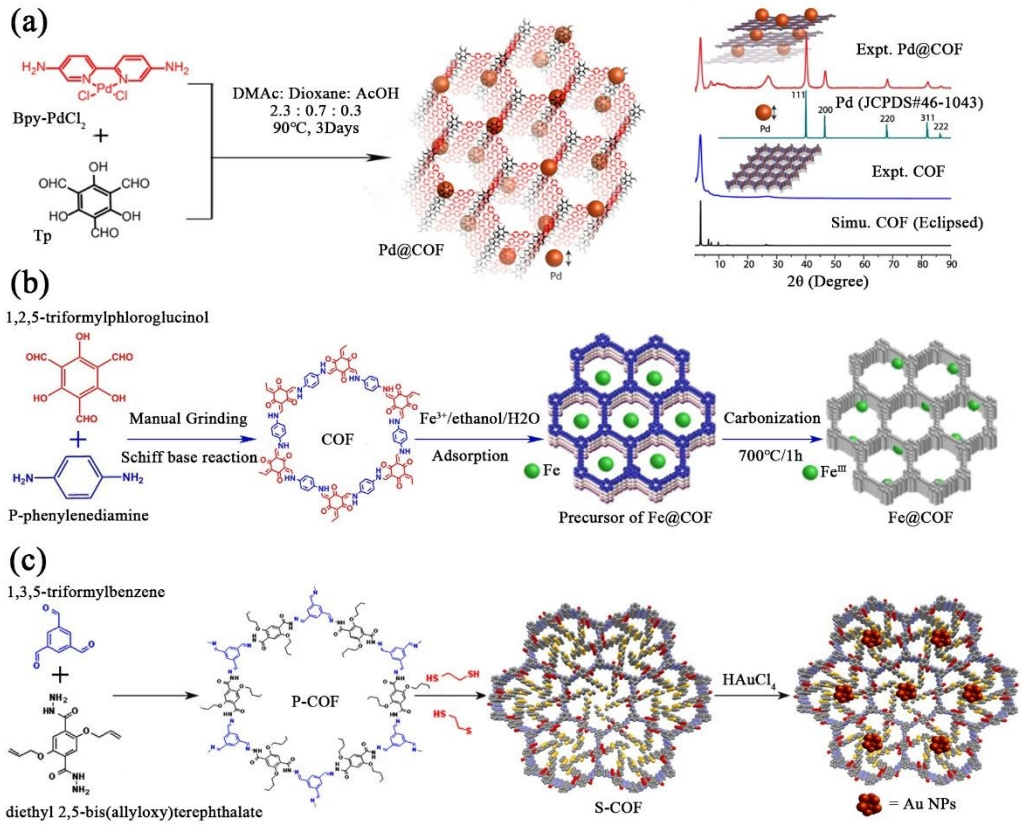

Fig. 2 (a) Left: synthesis details of the in-situ generation of highly dispersed Pd nanoparticles in the COF skeleton; right: comparison of PXRD patterns of simulated

View Article Online
DOI: 10.1039/D1TA04439G

COF (black) with experimental COF (blue), Pd nanoparticles (cyan), and experimental Pd@COF (red) (Reproduced with permission.[42] Copyright 2017, ACS Publications); (b) Illustrative procedure for the fabrication of Fe@COF catalysts (Reproduced with permission.[49] Copyright 2019, Elsevier); (c) Synthetic scheme of P-COF, S-COF and S-COF support to load gold nanoparticles (Reproduced with permission.[59] Copyright 2020, Elsevier).

3. COFs-confined catalysts

Different nano-scale catalysts (nanoparticles, nanoclusters, single atoms) have different interactions with COFs owing different building blocks (Table 1 and Fig. 3), thereby an accurate grasp of the relationship between them is the key to improving the catalytic performance of supported catalysts. At present, the research on the basic mechanism and structure of supported catalysts is still in the preliminary stage, so it is difficult to analyze them accurately by using conventional analytical methods. In 2008, F. Tao and G. A. Somorjai et al. used surface science and technology to study the structural reconstruction of reaction-driven Rh-Pd and Pt-Pd NPs,[64] revealed the questions related to the interaction between nano-scale catalysts and supporting materials and promoted the research process of the structure and reaction mechanism of supported catalysts. In this section, we summarize the recent reports of COF-confined catalysts, to understand the structural relationship between the active center and the carrier, to briefly describe the confinement effect of nano-scale particles in COFs.

Table 1 The interaction between nano-scale particles (nanoparticles, nanoclusters, and

View Article Online
DOI: 10.1039/D1TA04439G

241 single atoms) and COFs or COF-based materials in COFs-confined catalysts

COFs-confined catalysts	Loading(wt%)	Interaction	Refs.
Pd/Pt NPs@COF	34.36	The pores hold strong anchoring groups (thioether groups).	65
Au NPs@S-COF[a)]	24.00	Au-S-COF bond bridge.	59
Au NCs@COF-S-SH[b)]	N		43
Rh NPs@PC-COF[c)]	1.91	The accessible N sites in the pore can connect the nano-scale particles.	39
CdS NPs@CTF-1[d)]	19.3		48
Rh NPs@CTF	3.40		53
Pd NPs@TpBpy[e)]	15.20		42
Ni_3N NPs@COF	N		63
Pd NPs@COF	N		66
$Co/Co(OH)_2$ NPs@COF	16.00		67
Rh NPs@COF	4.00		68
Pd/Pt@CTF	0.10	The strong synergism between them enhances the adhesion energy of nano-scale particles.	45
Pd NPs@COF-SO_3H[f)]	0.38		50
Au NPs@TAPB-DMTP-COF[g)]	0.20	Encapsulation or modification of PVP/ZIF-8 to fix nano-scale particles in COFs pores.	61
Pd NPs@H-TpPa[h)]	N		62
Ru NPs@COF-ASB[i)]	4.10	Heteroatom functionalities (hydrazine) in support pores.	69
Pd NCs@COF-300-1114[j)]	1.10	Dangling amine groups on the support porous can confinement of ultrasmall NCs.	70
Cu NCs@CTF	4.80	The synergism between the two and the good chemical confinement environment.	71

View Article Online
DOI: 10.1039/D1TA04439G

Pd NPs@COF	5.00	Function bond (imine bond) in support pores.	72
Pd NCs@COF	N		73
Pt NPs@ sp^2c-COF[k)]	3.00	Interfacial charge transfer.	74
Pd@In NCs@N_3-COF	4.51 and 5.01		75
Pt atom@CTF	1.02	The rich-N sites of the support can accurately anchor single atoms.	76
Fe atom@COF	2.14		49
3d metal atoms[l)]@COF	N		77
Co atom@FPy-CON[m)]	2.10	Strong linkage of iminopyridine moiety.	78
TM atom[n)]@COF	N	The synergistic effect of TM single atoms and support.	79

[a)]S-COF: Sulfur-containing COF; [b)]COF-S-SH: A COF modified with thiol chains; [c)]PC-COF: Nitrogen - rich COF; [d)]CTF-1: A covalent triazine-based frameworks; [e)]TpBpy: COF material constructed by 1,3,5-triformylphloroglucinol (Tp) with 2,2′-bipyridine-5,5′-diamine palladium chloride (Bpy-$PdCl_2$); [f)]COF-SO_3H: A SO3H-anchored COF; [g)]TAPB-DMPT-COF: COF material constructed by 1,3,5-tris(4-aminophenyl)benzene (TAPB) with 2,5-dimethoxyterephthaldehyde(DMTP); [h)]H-TpPa: A active yolk–shell COF catalysts materials; [i)]COF-ASB: Condensation of benzene-1,3,5-tricarbohydrazide with benzene-1,4-dicarboxaldehyde generated a new COF; [j)]COF-300-1114: Tetrakis(4-anilyl)methane and terephthaldehyde (molar ratio=11/14) produced a dia-c5 topological COF; [k)]sp^2c-COF: with C=C bonds and afford fully p-conjugate frameworks; [l)]3d metal atoms: Mn, Fe, Co, Ni, and Cu; [m)]FPy-

View Article Online
DOI: 10.1039/D1TA04439G

CON: Fluorinated analogues covalent organic nanosheets; n)TM atoms: transition-metal atoms (Fe, Co, Ni, Mn, Cr, Ti……).

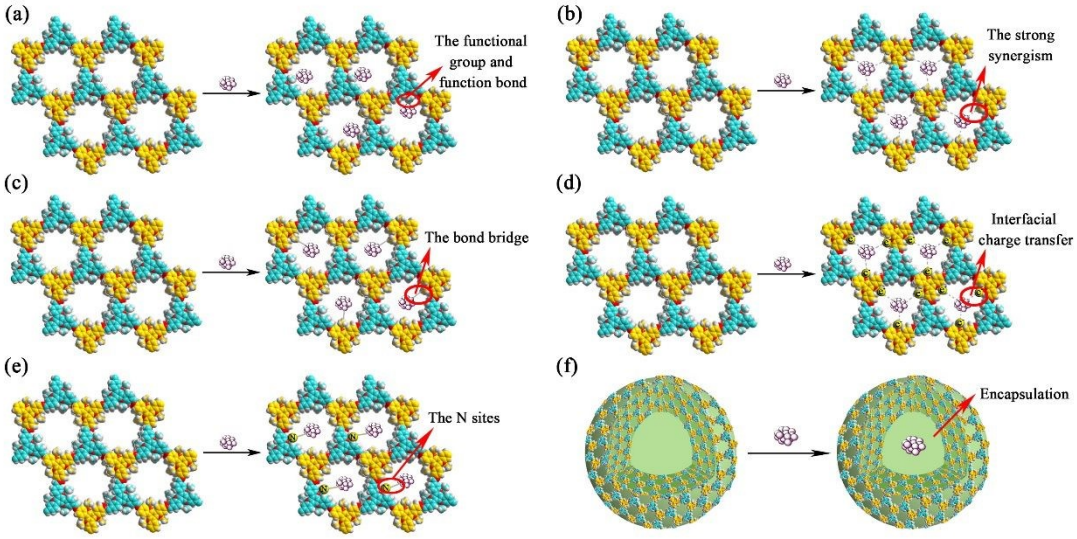

Fig. 3 The interaction between nano-scale particles (nanoparticles, nanoclusters, and single atoms) and COFs or COF-based materials in COFs-confined catalysts. (a) The pores hold strong anchoring functional groups and functional bond; (b) The synergistic effect of nano-particle and support; (c) Bond bridge can establish the interaction between nano-particle and support; (d) Interfacial charge transfer can establish the interaction between nano-particle and support; (e) The rich-N sites of the support pores can accurately anchor nano-particle; (f) Encapsulation can fix nano-scale particles in COF pores.

3.1 COFs-confined nanoparticles

Nanoparticles (NPs) are ideal candidates for heterogeneous catalysts due to their unique physical and chemical properties, such as large specific surface area, good stability, and many exposed active sites.[80, 81] However, NPs tend to agglomerate, which reduces their catalytic activity.[54, 82] However, NPs can be confined by porous supports,

View Article Online
DOI: 10.1039/D1TA04439G

enhancing catalytic active sites to improve the catalytic activity around them. As a new star of porous materials, COFs have excellent properties such as high surface, high porosity, and topological structure designability, showing their great potential as a support for NPs.[83-86] We found that the strong interaction between COFs or COF-based materials and NPs can reduce the Oswald ripening and spillover effect,[87, 88] and then improve the NPs dispersion and stability.

3.1.1 COFs-confined single-component nanoparticles catalyst

The unique porous organic framework in COFs materials is considered to be an important support for active metal NPs, and the rich nitrogen bond in the framework can better fix the metal NPs in the pores of COFs materials.[89, 90] The strong interaction between nitrogen bond and metal NPs can avoid the accumulation of NPs in the internal space of porous scaffolds and make them uniformly dispersed, thus improving the catalytic efficiency of COF-confined catalysts. Herein, Lu and co-workers synthesized a COF-based materials with high content nitrogen using piperazine and cyanuric chloride as raw materials.[39] The precisely designed N sites can interact with Ru ions to form Ru-N complexes (Fig. 4a). Ru ions could be reduced to Ru NPs in-situ, which was due to the adhesion energy of the interface between Ru NPs and COF-based materials, so that the reduced Ru NPs still could be confined in the pores of COF-based materials, which successfully prepared COFs-confined catalysts. This peculiar adhesion energy prevents the leaching and aggregation of Ru NPs to provide higher active sites. Apart from the above methods, NPs also can be immobilized through the interaction between metal surface and solvent. Ma and co-workers successfully synthesized palladium

View Article Online
DOI: 10.1039/D1TA04439G

291 nanoparticles (Pd NPs) and trapped them in the covalent pores of the CCOF according
292 to this strategy (using the interaction between chiral N-rich COF (CCOF) and palladium
293 nitrate solvents).[91] Related data showed that the combination of CCOF and Pd NPs
294 exhibit a special structure. According to the powder X-ray diffraction (PXRD) pattern
295 (Fig. 4b), it could be known that the synthesized Pd NPs were located between the
296 CCOF layers and N atoms in the layers. Through Barrett-Joyner-Halenda analysis, it
297 was found that the loading of NPs significantly changed the interlayer spacing of the
298 framework, and the optical property of the materials was improved, and the catalytic
299 performance of the catalyst did not decrease. Because NPs are embedded in COFs or
300 COF-based materials layers, the interaction between them made the interlayer distance
301 increase, thereby improving the absorption ability and catalytic performance. Islam and
302 co-workers successfully synthesized two COFs, which were modified with silver
303 nanoparticles (Ag NPs) on their outer surface.[54] COF-1 and COF-2 were the precursors
304 of COFs, and these COFs had abundant N centers and interacted closely with the outer
305 surface of Ag NPs according to density functional theory. The embedding of Ag NPs
306 not only unchanged the structure of COFs itself, but also optimized its catalytic activity.
307 Therefore, effectively confining the NPs into the pores of the COFs would help to build
308 a close cooperative relationship between the two to enhance the catalytic activity.

309 One of the common methods for embedding NPs into porous structures is the
310 interaction of the abundant nitrogen in COF or COF-based materials with NPs.[92] In
311 addition to N-rich COFs, a series of functionalized COFs (such as triazine, porphyrin,
312 pyridine, and imine etc.) can also effectively immobilize NPs into mesoporous structure.

View Article Online
DOI: 10.1039/D1TA04439G

For instance, N-rich carbon fiber COF is an ideal support for NPs.[93-95] The highly crystalline CTFs synthesized from triazine bonds contain abundant pyridinic nitrogen atoms (aromatic C=N), which can fix NPs.[95] In order to verify the effect of pyridinic nitrogen of CTFs on stabilizing metal NPs, Jin and co-workers used palladium and platinum NPs (Pd/Pt NPs) as representatives to design and prepare COFs-confined catalysts in a tunable CTFs platform.[45] This studies have found that pyridine nitrogen in CTF had a pair of isolated electron pairs, which could form a strong interaction with metal NPs and effectively control the size of metal NPs on a tunable CTFs platform. Among them, the instability of palladium leaded to higher interaction between Pd and pyridine nitrogen, which not only promoted the close connection between Pd NPs and CTFs support, to accelerate photoelectron transfer, but also helped to form smaller NPs. The experimental results shown that the interaction between Pd NPs and pyridine nitrogen is greater than that Pt NPs and pyridine nitrogen. Therefore, the catalytic performance of COFs-confined catalysts formed by Pd NPs interaction into CTF is better. The interaction between Pd/Pt and N was further verified and analyzed by x-ray photoelectron spectroscopy (XPS) (Fig. 4c). It can be known that the reason Pd NPs are uniformly dispersed in mesoporous CTF is that the ordered pyridine metal chelating center on the skeleton has a good immobilization effect on NPs, which further proves that the confinement effect formed by the strong interaction between CTF, and metal NPs is helpful to improve the catalytic performance.

The super-cage structure is used to fix nano-scale particles, and the controllable synthesis of ultra-fine NPs into large-size NPs is realized. The super-cage structure

View Article Online
DOI: 10.1039/D1TA04439G

makes the large size NPs stable, showing the stability of the encapsulation effect. Roeffaers and co-workers used electrostatic self-assembly of PVP in imine-based COFs to control the growth of metal NPs.[96] Since Pt NPs is usually charged, the use of insulator-terminated Pt NPs can effectively absorb light to excite hot π-electrons in imine-linked COFs and motivate photocatalytic reaction. In their work, by adding an insulator to imine-connected COF pores, the metal NPs are cleverly wrapped in the COF to achieve absolute stability of the metal NPs. It supplies a new guide for the advancement of the artificial optical system. To create new and attractive NPs loaded imine-linked COFs, many researchers explore other methods to limit NPs. Gu and co-workers synthesized the imine-linked COFs with thioether (Thio-COF) through a simple condensation reaction, in which the interaction between the functional groups of sulfides and NPs forms a bond bridge to improve the separation efficiency of photogenerated carriers.[65] The functional groups of thieother in the pore promote the close contact between the metal ion (Pt or Pd) and NPs through the metal-sulfur binding interaction, and the formed COFs-confined catalysts has excellent performance such as low loading, mild reaction condition, and high yield. The different interactions between COFs or COF-based materials and NPs form a variety of COFs-confined catalysts, which lays a foundation for the synthesis of multi-functional catalytic materials.

COFs or COF-based materials are formed by reversible covalent bonds, can in efficiency to stabilize metal NPs. In the presence of this covalent bond, it is easy to introduce heteroatom groups to connection of COF pores, such as imine, triazole, hydrazone etc. Then, the synergistic effect of these heteroatom groups and COF pores

View Article Online
DOI: 10.1039/D1TA04439G

can well confine NPs. A COFs-confined catalyst by hydrazone bonds to immobilize ruthenium nanoparticles (Ru NPs) with excellent catalytic properties was developed using Chen and co-workers.[69] The electronic differential system (EDS) mapping image and PXRD pattern respectively showed that Ru NPs were uniformly distributed in the hydrazone-linked COFs (Fig. 4d). The loading of Ru NPs had a good consistency with the hydrazone-linked COFs and showed that hydrazone was the link between COF and Ru NPs, which not only ensured the structural integrity but also improved the dispersion of NPs. The tunability of COFs not only allowed it to be modified by heteroatomic functional groups, but also could use post modification strategies to change A-COF to B-COF (A-COF and B-COF for different COF-based materials). Ding and co-workers took advantage of this performance to design and synthesize functionalized COFs.[59] Transforming the propylene functionalized COF (P-COF) to a sulfur-containing COF (S-COF), the rich thiol and thioether groups in the materials were used to anchor gold nanoparticles (Au NPs) to form Au-S-COF. The transmission electron microscope (TEM) directly showed the good dispersibility of Au NPs on S-COF (Fig. 4e), and high-resolution transmission electron microscope (HRTEM) displayed that the interplanar distance of Au NPs anchored on the surface of S-COF was 0.2nm, which reflected that the formed bond bridge provided more reaction spaces. However, not all modified COFs or COFs could produce strong interacting bond bridges with all active metals. In addition to using the form of bond bridge to strengthen the interaction between the two, Luo and co-workers proposed a new way to construct COFs that had a strong interaction with active metals.[50] This team meticulously designed -SO_3H (COF-SO_3H) anchored

View Article Online
DOI: 10.1039/D1TA04439G

COFs. Due to the presence of -SO_3H, the interaction between Pd NPs and COFs was enhanced (Pd/ COF-SO_3H), thereby reducing the size aggregation and spillover of Pd NPs. It could be seen from XRD patterns and scanning electron microscope (SEM) image that the loading of Pd NPs did not change the structure of COF-SO_3H and still maintained uniform fiber morphology. This was because the COF skeleton modified by-SO_3H could better adapt to the embedding behavior of Pd NPs by COF, which was closely related to the close interaction between the two. The interface sites around NPs were unique environment because they were can directly contact with supports and reactants to improve the stability of the catalyst. Hence, enhancing its interaction with COFs or COF-based materials is an important strategy to synthesize highly active catalysts.

In most cases, there is no interaction between scaffold lattice and NPs, thereby resulting in carrier defects or structural collapse. However, the heterogeneously nucleate can treat NPs as small insoluble particles dispersed in the solution, so that the COFs attaches to the nanoparticles to generate crystal nuclei.[97] Inspired by this, Zhu and co-workers reported a simple encapsulation technology to anchor PVP-modified Au NPs in 2D COF-based materials.[61] The surface of Au NPs was functionalized by PVP, which made Au NPs anchor on the surface of the synthesized COFs. It facilitated better adjustment of the composition, size, and shape of the nanoparticles. It was worth nothing that the modified Au NPs were first adsorbed on the COFs precursor instead of the heterogeneous nucleation. In a good environment, by the high surface energy of Au nanoparticles, the positive and negative of the particles are attracted to each other to

View Article Online
DOI: 10.1039/D1TA04439G

form a ball, which then effectively combines with the COF precursor. TEM measurements showed that the central area of each aggregated ball (COF-based materials) contained several Au NPs (Fig. 4f). Control experiments showed that COFs had no reduction performance, and its main reaction site was the surface of active Au NPs. The similar strategy of using COFs as a shell to encapsulate metal NPs attracted the attention of Li and co-workers.[98] They introduced a self-template ZIF-8 core-shell nanostructure as the support of metal NPs to synthesize COFs-confined catalysts. The ZIF-8 modified metal NPs were encapsulated into COFs cavity, and ZIF-8 could be etched away during the formation of COFs to expose active sites. In addition, the sacrificial template also could enhance the permeability of the COFs shell of the outer porous structure, allowing the reactants to fully contact with metal NPs, thereby enhancing the synergistic effect between supports and metal NPs. It is worthy of our attention that this synthesis strategy is suitable for confining a variety of NPs, and can it easily change and adjust the function and performance of the catalyst.

3.1.2 COF-based multi-component nanoparticles catalyst

As mentioned above, the single-component NPs can form a strong interaction with special sites in COFs (such as N sites,[53] triazine group,[99] hydrogen-bonded phenolic group,[100] and amine groups.[101]), thereby forming high-stability COFs-confined catalysts. It is because the single-component NPs and COF or COF-based carrier form a strong interaction to improve the dispersibility of single-component NPs. However, most of the single-component NPs are noble metals, resulting in high cost and it is not suitable for mass production. Therefore, finding multi-component NPs with reasonable

View Article Online
DOI: 10.1039/D1TA04439G

price and simple preparation process is very important for practical application. Zou and others discovered a semiconductor material that can replace single-component NPs-CdS (cadmium sulfide), which had the advantages of strong photoelectric effect, simple preparation, and low price.[48] Using CTFs to anchored CdS NPs, the strong metal-nitrogen interaction in CdS-CTF prevented CdS NPs from photo-corrosion and aggregation, and XRD patterns showed that the addition of nanoparticles did not change CTFs structure. (Fig. 4g). Wherefore, the superior photocatalytic performance of the composite material was attributed to the formation of smaller CdS NPs in the pores of CTF, which not only maintained the original crystal structure of CTF, but also exposed more active centers. Anchoring CdS NPs on COFs also had been reported by Kurungot and co-workers,[102] they adopted a highly stable 2D-COFs as the support of CdS NPs and used the π-π superimposed interaction in 2D-COFs to form a sheet layer, and CdS NPs could be evenly distributed in the COFs flake matrix. Mott–Schottky (MS) and photoluminescence (PL) showed that the strong interaction between 2D-COF support and CdS NPs not only effectively inhibited the recombination of photogenerated electrons-hole pair (Fig. 4h), but also improved the light stability of NPs, so that the nanocomposite had higher catalytic activity.

Immobilization of multi-component NPs on the support to enhance its stability and control its spatial distribution is the most effective way to improve the catalytic performance of NPs. However, the support usually not inert, and the interaction with NPs will produce new interface phenomena. R. Vaidhyanathan and co-workers synthesized strategically positioned -OH and N-rich COF.[63] This type of COFs

View Article Online
DOI: 10.1039/D1TA04439G

interacted strongly with Ni_3N NPs, limiting the size of the Ni_3N NPs to <2 nm. Surprisingly, the growth sizes (3-5nm) of a few Ni_3N NPs were higher than the limit aperture of COFs (27.0 Å), but they were still smaller than naked Ni_3N NPs (18-20 nm). These NPs growth size than the supports pores, thereby generating new boundary phenomena in the catalytic system. Some interface phenomena promote NPs loading, and some will produce Oswald ripening phenomenon, especially in larger NPs. In 2018, the author led a new team to elaborate on this interface phenomenon,[67] which adopted COF-based materials as support to confine larger $Co/Co(OH)_2$ NPs, the N-rich binding pocketed in COFs ensured the strong interaction between $Co/Co(OH)_2$ NPs and COFs (Fig. 4i). These nitrogen bonds could make $Co/Co(OH)_2$ NPs stable in COFs matrix, so that the $Co/Co(OH)_2$ NPs are not filtered out. The synthesized COFs composite was modeled by some characterization methods such as DFT calculation and Brunner−Emmet−Teller (BET), high resolution transmission electron microscope (HR-TEM), all of them revealed that COFs were used as porous scaffolds, and the size of $Co/Co(OH)_2$ NPs exceeds the supports pores. The authors further studied the effect of the exposed surface of NPs on the heterogeneous catalytic system by calculating the energy associated with the activation of the reactants and substrates. The calculation results revealed that the complex could modulate the catalytic activity through the specific exposed surface of the NPs. These works can give us a better understanding of the interaction between NPs and COF-based materials, which can highlight the great potential of COFs as a carrier for the synthesis of high-efficiency catalysts.

View Article Online
DOI: 10.1039/D1TA04439G

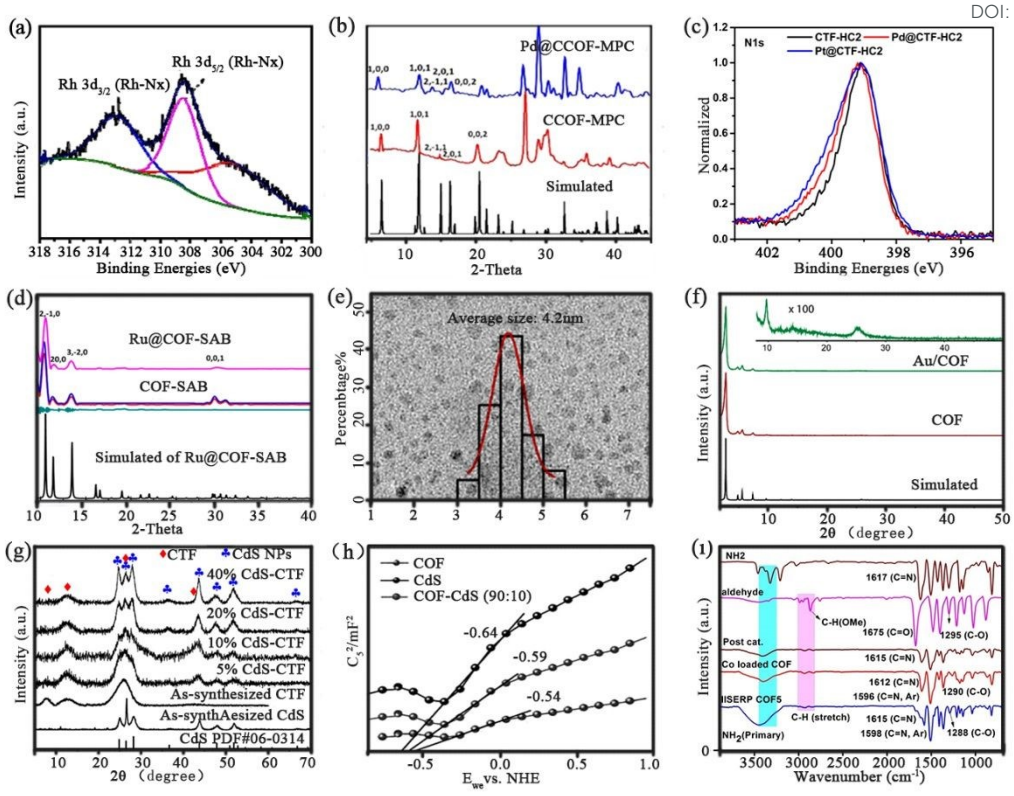

466

467 **Fig. 4** (a) XPS spectra of Rh 3d peak for 1.91 wt.% Rh-N/PC-COF (Reproduced with
468 permission.[103] Copyright 2020, Poyal Society of Chemistry); (b) Simulated and
469 measured PXRD patterns of Pd@CCOF-MPC and CCOF-MPC(Reproduced with
470 permission.[104] Copyright 2017, ACS Publications); (c) XPS N1s peaks for CTF-HC_2
471 (Reproduced with permission.[45] Copyright 2020, ACS Publications); (d) The simulated
472 (black line) and measured PXRD patterns of Ru@COF-SAB (red line) and COF-SAB
473 (purple). Riveted refinement (blue line), and the difference plot between measured and
474 Rietveld-refined PXRD patterns (dark green line) (Reproduced with permission.[69]
475 Copyright 2018, ACS Publications); (e) The TEM image of Au-S-COF, the insert
476 histogram is distribution of Au nanoparticle size (Reproduced with permission.[59]
477 Copyright 2020, Elsevier); (f) Powder XRD patterns for as-synthesized COF and COF

View Article Online
DOI: 10.1039/D1TA04439G

composite containing of 0.20 wt % 15 nm Au NPs and simulated XRD pattern for TAPB-DMTP-COF. Inset is the same XRD pattern for the Au/COF composite but with the adjusted intensity scale, where weak peaks associated with diffraction of COF can be observed but those assignable to Au NPs cannot (Reproduced with permission.[61] Copyright 2017, ACS Publications); (g) XRD patterns of the as-synthesized samples (Reproduced with permission.[48] Copyright 2020, Elsevier); (h) Mott–Schottky plots of COF, bulk CdS, and CdS-COF (90:10) hybrids (Reproduced with permission.[102] Copyright 2014, Britannica); (i) Monomers, and the IISERP-COF5. The highlighted regions indicate the peaks in the COF due to the unreacted terminal aldehyde/amine functionalities (Reproduced with permission.[67] Copyright 2018, Wiley Online Library).

3.2 COFs-confined nanoclusters

Nano-scale particles vary in size, they will exhibit different catalytic behavior from the traditional catalysts, because the nanoparticles are affected by the quantum size effect, that is, the smaller the size is, the greater the surface energy of the NPs have.[61, 105, 106] When the diameter of the nano-scale particles is less than 1 nanometer, they are called nanoclusters (NCs). Their higher surface energy makes the particles in an active state, resulting in poor stability and low catalytic performance.[62] In order to increase the surface energy of the material, the researchers discovered a new COF-based materials containing thiol chains (COF-S-SH), in which -SH groups used as nucleation sites to form strong S-Au bonds with gold NCs (Au NCs) to improve stability of catalysts.[43] The strong metal-support interaction (-SH groups anchored Au NCs to form Au-S-COF bonding bridge (Fig. 5a) not only improved the surface adsorption energy

View Article Online
DOI: 10.1039/D1TA04439G

of carbon nanotubes, but also promoted the growth of ultra-fine Au NCs, thereby improving the separation of electrons and holes. Generally, most of the NCs anchored on COFs support cannot be efficiently introduced into the pores, and only a small part of NCs is embedded in the support. [107] In order to solve this problem, Guo and co-workers used nonstoichiometric synthetic strategy to efficiently limit the amine functional groups to anchoring platinum NCs (Pd NCs).[70] It could be clearly seen from XRD spectrum that Au NCs had no diffraction peaks, writing down that the growth of Au NCs was well controlled by the COFs pores (Fig. 5b), thereby resulting in a small size of NCs. Furthermore, Zou and co-workers found that COFs or COF-based materials had high porosity and good molecular sieving performance, and COFs-confined catalyst was successfully synthesized by using these characteristics.[71] The X-ray absorption analyses revealed that copper NCs (Cu NCs) were embedded in bipyridine-modified CTF materials (Fig. 5c). The inductively coupled plasma optical emission spectrometry (ICP-OES) showed that CTFs with triazine ring could not effectively anchor Cu NCs, while the addition of bipyridyl groups could enhance the interaction between CTFs and Cu NCs. Therefore, CTFs could provide a good environment to stabilize Cu NCs through pre-designed bipyridine organic ligands and porous framework structures. In addition, metal ions could be first adsorbed by special functional groups in building blocks and then reduced into NCs in-situ. Liang and co-workers found a COF with imine bonds, which could adsorb palladium ions (Pd^{2+}) to form a Pd^{2+}-COF complex.[73] Pd^{2+} ions adsorbed on the surface were reduced to Pd NCs on COF supports. The strong interaction between the imine bond and Pd NCs confine

View Article Online
DOI: 10.1039/D1TA04439G

the growth of the Pd NCs, thereby improving the dispersion of Pd NCs. This strategy not only adjusts surface the electronic structure of Pd NCs/COF, but also increases the active sites, thereby improving the catalytic effect and stability of Pd NCs/COF. It was no doubt that the porous structure of COFs provided binding sites for different NCs, so that these nanoclusters could be stably and evenly distributed on the pores. Therefore, it is extremely important to understand the relationship between support structure and active site.

The synthesis of COFs-confined catalysts for heterogeneous catalysis using multi-component NCs as the active sites, but the growth of NCs also brings great challenges. Recently, P. Kour and S. P. Mukherjee reported a perovskite NCs of $CsPbBr_3/Cs_4PbBr_6$@EB-COF: Br (EB-COF: Br is Br-functionalized COF).[108] The authors used Br-functionalized COF as an encapsulation material to control the synthesis of perovskite ($CsPbBr_3/Cs_4PbBr_6$) NCs, which had chemical affinity and non-interference with the photoluminescence of brominated perovskite. It not only reduces the toxicity of lead (Pb) in the system, but also improves the stability of the $CsPbBr_3/Cs_4PbBr_6$ NCs. COFs and COF-based materials plays lot of roles in COFs-confined materials. In addition to a support, COF also can be used as a photosensitizer to improve the light response. Lu et al. used photosensitizing N_3-COF to limit the growth of bimetallic Pd@In NCs and simultaneously catalyze the reduction of CO_2 to alcohols.[75] The authors indicated that a strong interaction (internal electron transfer) was existed in Pd@In nanostructure, and there were some synergies (external electron transfer) between Pd@In NCs and N_3-COF, which greatly contributed to C–C coupling

View Article Online
DOI: 10.1039/D1TA04439G

and interfacial charge transfer. This work highlights the fact that bimetallic NCs are confined into photosensitizing supports that rely on charge transfer between their face, thereby improving the efficiency of photosynthesis.

3.3 COFs-confined single-atom

The size effect in the confinement effect is the most important factor in our discussion of the relationship between supports and nano-scale particles. For nano-scale particles, their electronic structure and geometric structure will change with the change of size especially single-atom catalysts with a size smaller than 0.1 nm.[4] Hence, the single-atom catalysts have attracted great interest in the field of catalysis due to their unique structure,[109] which not only shows the advantages of heterogeneous catalysts, but also keeps the performance of homogeneous catalysts. The single-atom catalyst is a catalyst in which the metal component is interdependent with non-porous or microporous/mesoporous materials in the form of single atom, and the surface reaction is simple. However, it is difficult to control the leaching rate of single atom in synthesis and reaction process.[110] Whereas, as a recent material star, COFs have periodic and permanent porosity, which can well accommodate single active site and effectively transform photogenerated charges to active sites.[71] In addition, compared with support-based single-atom, COF-based single-atom shows superior porous structure, which can display better performances. In this section, we summarize the potential of different COFs and COF-based materials to fix different single metal atoms.

3.3.1 COF-based noble single atom

A class of interesting macrocyclic ligands containing N-containing were reported

View Article Online
DOI: 10.1039/D1TA04439G

by Zhu et al.[53, 111, 112] They had rich coordination chemistry and could anchor noble single atom. When noble metal atoms are used as the active center of the catalyst, nitrogen sites are used to stabilize noble metal atoms. Huang and co-workers successfully synthesized CTF with rich in N_3 group.[76] The Pt single-atom are anchored on CTF by -N_3 sites, thereby effectively controls the growth of Pt single-atom in adsorption (Fig. 5d). In addition, COF also can bond to -N site to form CTF in addition to bond with -N_3 site. Nakanishi and co-workers have prepared CTFs-supported Ru single atom, where Ru atoms were connected by -N to form Ru-N coordination bonds.[89] In cyclic catalytic reaction, Pt and N atom bonded in CTFs to form a tight connecter Pt-N bond unchanged, but Ru-N bond was oxidized and transformed to a high-valency oxide Ru=O. Although Ru atom-modified CTFs was oxidized to high-valency Ru=O, it was highly stable during the long-term electrolysis in an aqueous solution. The choice of monatomic species has a great influence on the success synthesis of COFs-confined catalysts, and the strong metal support relationship is the key to material synthesis. For supported precious metal catalysts, the embedding of precious metals often stop the active sites from blocking, because the precious metals can accurately combine with fixed anchor points, thus reducing the effect of single atom embedding on the support.

3.3.2 COF-based non-noble single atom

The large-scale development of precious metals as active centers had a fatal disadvantage since that the reserves of precious metals on the earth is very low and the durability of catalysts is poor, which seriously hinders the large-scale production of catalysts. To meet the needs of society, non-precious metals, as a widespread species

View Article Online
DOI: 10.1039/D1TA04439G

on the earth, have become a research hotspot in the development of low-cost and high-efficiency catalysts. When a non-noble single atom is embedded into a porous material (COFs or COF-based materials), the single atoms usually replace the heteroatoms (such as N, S, O etc.) or occupy the vacancy formed by other atoms on the supports, so that the atoms can grow and fix well in the porous materials, and then improve stability of catalysts.[35, 113] In recent years, as a kind of microporous polymer, COFs can anchor most non-noble single atoms. The main reason is that they have a large number of heteroatoms and lone electron pairs to anchor metal atoms through coordination bonds.[67] Based on the characteristics of COF-based materials, Kamiya and co-workers studied the relationship between the 3d non-precious metal (Mn, Fe, Co, and Cu) and COFs through hard exploration and long-term research (Fig. 5e).[77] This team established the metal center and N atom model and revealed that a stronger target absorption was achieved when there were fewer d-electrons. By comparing some models such as M-N_4 (coordination number = 4), M-N_3 (coordination number = 3), and M-N_2 (coordination number = 2), they drew a conclusion that the smaller coordination number had stronger adsorption. The non-noble single atom with smaller d-electrons and coordination number can combine well with oxygen molecules in COFs-confined catalysts (according to the theoretical calculation system, Fe and Co-N_4 had high catalytic activity, while Cu and Ni had poor catalytic performance because of their weak interaction with oxygen molecules). It can be seen that Fe and Co have strong interaction with the support, which can significantly enhance the adsorption of reactants and the shedding of products during charge transfer. Therefore, the single atom can be

View Article Online
DOI: 10.1039/D1TA04439G

closely combined with the carrier to achieve the purpose of uniform dispersion by property adjusting the d electrons or reducing the coordination number. The dispersion of single atom in COFs-confined catalysts is inseparable from the strong interaction between carrier and single atom, and the weak interaction easily leads to atomic leaching to reduces the practicability of the material.

Although COFs with a multimeric pore structure can provide a clear and coordinated environment to accommodate a non-noble single atom, the instability of the binding site between metal and support and the existence of non-uniform defects on the support surface result in low loading and uneven distribution of metal atoms.[114] Therefore, the load and dispersion of metal atoms by accurately designing the loading sites of metal atoms can be increased. Chen and co-workers used the pyridine units and their adjacent imine groups as the bridge to connect single cobalt (Co) atom and COFs,[78] realizing the precise control of the spatially arranged catalytic sites on the surrounding chemical environment. HAADF-STEM indicated that Co atoms were uniformly distributed on the COFs matrix and Fourier transform infrared (FT-IR) indicated that structure of COFs did not change during the delamination and metal loading process (Fig. 5f). Therefore, it is of great practical significance to embed the active site in the pore purposefully under a certain chemical environment. Wang and his colleagues also tried to synthesize functional COFs by using bipyridine functional groups with strong adsorptive.[56] The synthesized functional COFs not only improved the stability of single metal atoms, but also established donor-acceptor channels with intramolecular electron delocalization and cascade effects with single metal atoms. It

View Article Online
DOI: 10.1039/D1TA04439G

632 was because the -C=C- bridging in the sp^2c-COF_{dpy} connected the donor-acceptor
633 channel of intramolecular electron delocalization and cascade effects. From the
634 perspective of sunlight utilization, bipyridine instead of biphenyl skeleton acted as an
635 electron acceptor through intramolecular interaction to realize electron transfer in this
636 system, thereby improving sunlight utilization. Additionally, according to the Kubelka-
637 Munk equation, the band gap of sp^2c-COF_{dpy} was calculated to be 2.03 eV. Therefore,
638 this catalytic system can efficiently utilize solar energy and has higher catalytic activity,
639 thereby laying a good foundation for the development of COF-based materials.

640 It is well known that the spatial arrangement of active metal centers is precisely
641 manipulated in an ordered organic framework through the combination of organic
642 couples. However, Gao and colleagues integrated the activated metal center into COFs
643 or COF-based materials that contain special functional groups, and successfully
644 synthesized a COFs-confined catalyst with excellent performance.[115] The main body of
645 the material was constituted by phthalocyanine borate COFs and Co atoms, Co atoms
646 represented active metal sites and they were loaded into the phthalocyanine block
647 before synthesizing COFs (Fig. 5g). Since the electronic structure of synthesized
648 catalyst essentially affect the efficiency of catalyst. The general characteristics of COFs
649 was explained though the projected density of state (PDOS). The results showed that
650 the 2p orbitals of four nearest nitrogen atoms in Co atoms and Co 3d orbital had a strong
651 resonance, and the energy level of Co 3d orbital in the phthalocyanine was higher than
652 that of the porphyrin. The stronger crystal field enhanced the combination of Co and
653 phthalocyanine and improved the stability of the material. The use of functional COFs

View Article Online
DOI: 10.1039/D1TA04439G

to anchor non-metal single atoms provides a reasonable way to optimize the catalytic performance of COF-based materials, which has attracted considerable attention. In order to build an efficient catalytic system, Yao and co-workers had proposed a new strategy to prepare COF-confined catalysts, which exhibited outstanding catalytic efficiency and strong durability in acidic and alkaline media.[49] This team used the abundant pyrrole nitrogen of COF as adsorption site for single metal atom, and the EDS mapping showed that Fe, N, O, and C elements were evenly dispersed on the support (Fig. 5h). The COFs and Fe-embedded COFs are analyzed through field emission SEM (FE-SEM) images. It can be known that the structure of COFs remained unchanged before and after Fe doping, and it could be clearly observed that there was no agglomeration of Fe atoms in the pores of the COFs. In addition, the abundant and stable nitrogen atoms in COF had a strong interaction with the optimized single atoms, which made COFs-confined catalyst exhibit excellent catalytic performance. Inspired by the high-efficiency catalyst for the synthesis of 2D polymerized phthalocyanine with embedded iron atoms, Zhao and co-workers successfully synthesized COFs with phthalocyanine and pyridine bond,[79] and the first principles proved the firmness of COF-based materials for anchoring transition metal (TM) atoms (TM-COF). According to the binding energy (E_b) value range of TM-COF (-3.44 to -9.43 eV) (Fig. 5i), TM atoms were uniformly fixed in the pore of COFs to avoid their migration and leach, thereby promoting electron transfer, and increasing reactive sites. The COFs-confined single atoms catalysts not only provide a new catalytic system, but also open a new chapter for the development of controllable multifunctional catalysts.

View Article Online
DOI: 10.1039/D1TA04439G

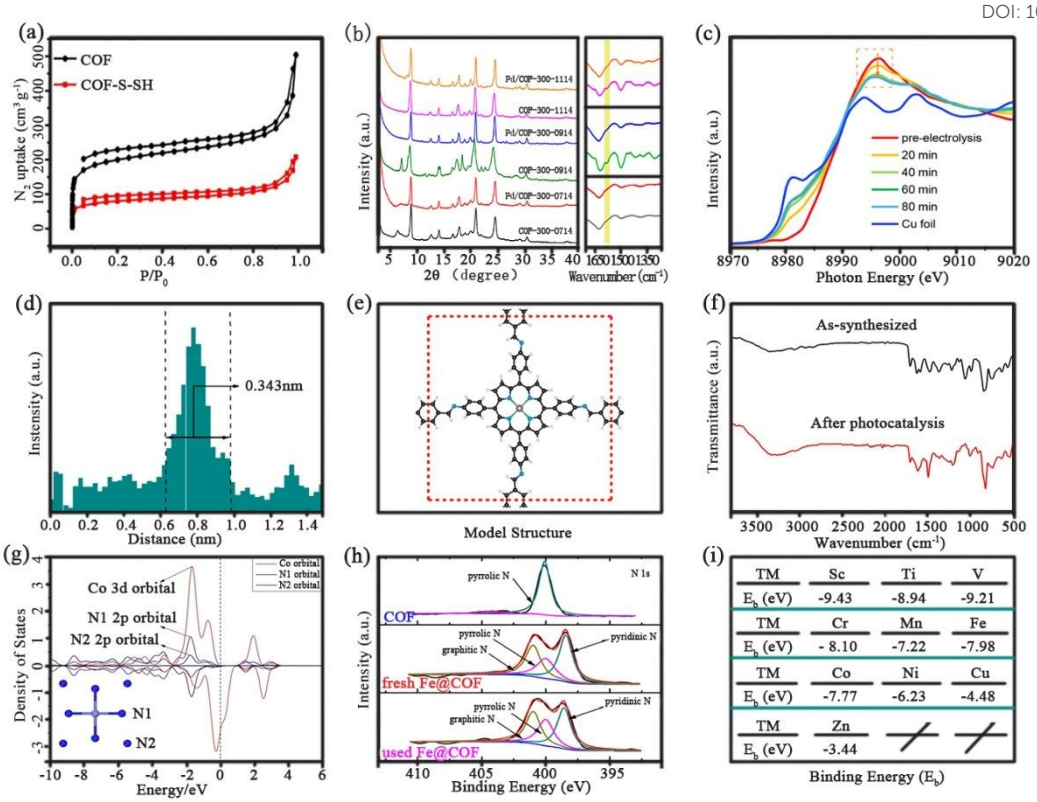

Fig. 5 (a) N_2 adsorption isotherms of COF and COF-S-SH (Reproduced with permission.[43] Copyright 2020, Wiley Online Library); (b) Comparison of XRD patterns and FT-IR spectra of Pd/COF-300-xy and COF-300-xy (xy = 0714, 0914, and 1114) (Reproduced with permission.[70] Copyright 2020, ACS Publications); (c) Real-time operando XAS measurements of CTF-Cu-4.8% at −1.45 V vs SHE (Reproduced with permission.[71] Copyright 2020, ACS Publications); (d) The corresponding intensity profiles for the atomically dispersed single Pt atom (Reproduced with permission.[76] Copyright 2020, ACS Publications); (e) Model structure employed in this study, porphyrin-type unit cell (M−N4) after structural optimization. Gray: transition metal atoms (M); black: C; white: H; blue: N. The red dotted lines represent the unit cell for each structural model (Reproduced with permission.[77] Copyright 2020, ACS Publications); (f) FTIR spectra of Co-COF before (black) and after (red) photocatalysis

View Article Online
DOI: 10.1039/D1TA04439G

(Reproduced with permission.[78] Copyright 2020, ACS Publications); (g) Projected density of states of Co-COF. The inset shows the crystal field around the Co atom (Reproduced with permission.[115] Copyright 2018, Britannica); (h) High-resolution XPS spectra, fresh and used Fe@COF catalysts (Reproduced with permission.[49] Copyright 2019, Elsevier); (i) Binding Energy (Eb) for transition state elements (Reproduced with permission.[79] Copyright 2020, ACS Publications).

4. Heterogeneous catalytic reaction

The efficiency of heterogeneous catalytic reactions is closely related to catalytic materials. With the development of supported catalysts, different confined catalysts have been found in electrocatalysis, photocatalysis, and other fields. From Table 2, we can clearly understand the wide application of COFs-confined catalysts. In this part, we discussed the application of different types of COFs-confined catalysts in heterogeneous catalytic reactions (Table 3) and selected some representative reactions that have attracted attention in practical applications to reflect the catalytic performance.

Table 2 Comparison of catalytic performance of COFs-confined catalysts, MOFs-confined catalysts, and zeolites-confined catalysts in practical applications.

Catalytic property	COFs-confined catalysts	MOFs-confined catalysts	Zeolites-confined catalysts
Stability	High	Low	High
Confinement effect	Strong	Moderate	Strong
Shape electivity	Yes	Limited	Limited
Scope of reactions	Suitable for all reaction conditions	More suitable for reaction under mild Conditions	Widely used for conventional thermal catalysis

706 **Table 3** Summary of typical works on photo(electro)catalytic application of COFs-confined catalysts

Application	Catalysts	Synthesis method	Reaction environment	Performances	Refs.
Hydrogen production	CdS NPs@CTF-1 (photocatalysis)	Impregnation combined with photo-deposition approach	An aqueous solution containing 8 ml lactic acid	H_2 evolution rate of 11.43 mmol g^{-1} h^{-1}	48
Hydrogen production	Pt NPs@COF (electrocatalysts)	Solvothermal and invasion deposition methods	Ag/AgCl as conducted, graphite as electrode in $NaHCO_3$ electrolyte	H_2 produced is 13 times higher than that of Pt/C on the market and FE[a)] is 100%	96
Hydrogen production	CdS NPs@COF (photocatalysis)	Hydrothermal synthesis methods	An aqueous solution containing lactic acid and 0.5 wt% Pt	H_2 evolution rate of 3678 mmol g^{-1} h^{-1}	102
Hydrogen production	Pt NPs@TP-COF (photoelectrocatalysis)	An electrostatic self-assembly method	The efficient hot π-electron tunneling of organic MIS[b)] nanostructures	H_2 evolution rate of 8.42 mmol g^{-1} h^{-1} and a TOF[c)] of 789.5 h^{-1}	93
Hydrogen production	Pd NPs@CTFs (photocatalysis)	Solvothermal and in-situ deposition methods	An aqueous solution containing 10 mL TEOA[d)]	H_2 evolution rate of 10.556 mmol g^{-1} h^{-1}	45

Hydrogen production	Rh NPs@PC-COF	Ultrasonic impregnation reduction and in-situ reduced method	1 mL of MeOH[e)] and DCM[f)] mixture solvent (V_{MeOH}/V_{DCM}=2/1)	The total TOF of 505 min^{-1} at 298 K	103
Hydrogen production	Pt NPs@ sp^2c-COF (photocatalysis)	Solvothermal andin situ photodeposition method	An aqueous solution (100 mL) containing triethanolamine (10 vol %)	H_2 evolution rate of 1360 μmol h^{-1} g^{-1}	74
CO_2 reduction reaction	Ru NPs@TpPa-1[g)] (photocatalysis)	Solvothermal synthesis method	In a mixture liquid of MeCN[h)] and TEOA with a volume ratio of 10:1	HCOOH evolution rate of 108.8 μmol $g_{cat}^{-1}h^{-1}$ (3.0 wt% Ru)	116
CO_2 reduction reaction	Pd@In NCs@N_3-COF	Solvothermal synthesis method	CO_2 photoreactor containing ≥ 99.995%	Total yield of 798 μmol g^{-1} for producing CH_3OH (74 %) and CH_3CH_2OH (26 %)	75
CO_2 reduction reaction	Co atoms@sp2c-COF_{dpy} (photocatalysis)	Solvothermal and impregnation deposition	An aqueous solution containing 5 mL TEOA	Achieving up to 17.93 mmol g^{-1} CO with 81.4 % selectivity in a long-range reaction	56

CO_2 reduction reaction	Cu atoms@CTF (electrocatalysis)	In-situ oxidation method and wet-impregnation method	In an airtight H-type electrolytic cell, which adopts a three-electrode system to constant potential electrolysis	At a potential of −1.3 V, CO and H_2 are the main gas products	71
CO_2 reduction reaction	Co atoms@FPy-CON (photocatalysis)	Solvothermal and infiltration deposition method	An aqueous solution containing 2,2′-bipyridyl, acetonitrile and TEOA	CO production of 10.1 μmol (6 h irradiation under visible light) and CO/H_2 selectivity of 76%	78
Reduction of 4-nitrophenol	Au NPs@TAPB-DMTP-COF	Solvothermal and encapsulation method	An aqueous solution containing 4-nitrophenol and $NaBH_4$	Apparent rate constant *k* of 0.12 min^{-1}	61
Reduction of 4-nitrophenol	Pt NPs@Thio-COF[i)]	Solvothermal and impregnation deposition	An aqueous solution containing 4-nitrophenol and $NaBH_4$	The full conversion of 4-nitrophenol to 4-aminophenol in 8 min	65
Reduction of 4-nitrophenol	Au NPs@S-COF	Synthesis strategy of solvothermal and post-modification	An aqueous solution containing 4-nitrophenol and $NaBH_4$	The full conversion of 4-nitrophenol to 4-aminophenol in 7 min	59

Henry reaction and reductive Heck reaction	Pd NPs@CCOF-MPC[j)]	Solvothermal and sequential solution impregnation	An ethanol solution containing Ar-CHO, and nitromethane; An ethanol−H_2O solution containing 2-cyclohexen-1-one, and Ar-X	TON[k)] and TOF are 48.5 and 6.1 h^{-1}, respectively; TON and TOF values for the reaction are 30.9 and 3.09 h^{-1}, respectively.	104
Organic reaction	Ru NPs@COF-ASB	Solvothermal and impregnation deposition	A mixture of benzyl alcohol and corresponding amine	TON and TOF of N-benzylideneaniline formed from alcohol and amine were 18 and 0.82 h^{-1}	69
Organic reaction	Pd NCs@COF-300-1114	Nonstoichiometric synthon strategy and solvothermal condensation method	The oxidation reactions of benzyl alcohol under 0.1 MPa of O_2 at 90 °C in toluene	97.0% conversion of benzyl alcohol and 97.0% selectivity to benzaldehyde after 32 h	70
Organic reaction	Pd NPs@TpBpy	Solvothermal and in-situ deposition	Solution containing 2-bromophenol and terminal alkynes	The synthesis of 2-substituted benzofurans from 2-bromophenols and terminal alkynes	42
Organic reaction	Ag NPs@TpPa-1 and Ag NPs@TpTta[l)]	One-pot Polycondensation and infiltration deposition	Solution containing allylamine, strong iodinating agent NIS[m)] and DMSO[n)]	Synthesis cyclic carbamate 2a the catalyst in high yield of 96%	54

Organic reaction	Rh NPs@COF	Facile hydrothermal method	Solution containing 7.2mmol aromatic aldehydes and 3 mL 2.0 mol/L methanol of ammonia	Benzaldehyde with the full conversion of 99% and selectivity of 95% for Nbenzylidene(phenyl)methanamine	68
Organic reaction	Pd NPs@COF	Solvothermal and post-modification method	Solution containing aryl halide, aryl boronic acid, alkalic additive Cs_2CO_3 and solvent EtOH under N_2 atmosphere	Succeed in synthesizing halo-substituted beryl products in excellent yield	66
Organic reaction	Ru atoms@CTF (electrocatalysis)	Solvothermal method	Ag/AgCl and titanium wire used as reference electrodes and counter electrodes	Gaseous ethylbenzene oxidized to acetophenone	89
Oxygen reduction reaction (ORR)	TM atoms@COFs (electrocatalysis)	The VASP[o)] calculations of the density functional theory	N/A	Mn-COF and Cr-COF ORR overpotentials of 0.31 and 0.29 V, respectively	79
Oxygen reduction reaction (ORR)	3d metal atoms@COFs (electrocatalysis)	Systematic design of catalysts using first principles	N/A	Fe or Co−COFs are already known as efficient ORR catalysts	77

Hydrogenation reaction	Pd NPs @COF-SO_3H	Wet-chemistry immersion dispersion method	Under mild reaction conditions (1 bar of H_2, 25 °C, 28 min)	The selective hydrogenation of phenylacetylene with 97.06% conversion	50
Hydrogenation reaction	Pd NPs@COF	Static precipitation after ultrasonic treatment	An aqueous solution containing 5 mL (25 μL mL^{-1}) nitrobenzene in ethanol under 1 bar H_2	TON for the hydrogenation of nitrobenzene was 906 h^{-1}	72
Organic pollutant degradation reaction	Au NCs@S–COF[p)] (photocatalysis)	Solvothermal and post-modification strategy	An aqueous solution (50 ml) containing Rhodamine B (10 mg/L) or Bisphenol A	Rhodamine B and Bisphenol A degradation percentage of 97.3% and 90%	43
Organic pollutant degradation reaction	CsPbBr3/Cs4PbBr6 @EB-COF: Br[q)] (photocatalysis)	A simple mechanochemical synthetic	Various concentrations of MO[r)] aqueous solution (20, 50 and 100 ppm)	MO in aqueous media with a photodegradation rate of about 0.245 min^{-1}	108
Organic pollutant degradation reaction	Au NPs@COF	Solvothermal and post-modification strategy	Solution containing 12 mg/L 4-NP (25 mg/L for cong red and methylene blue)	With high flux (2000 L $m^{-2}h^{-1}$) and excellent reduction efficiency (more than 99%)	117

Nitrogen reduction reaction (NNR)	Mo atoms@Pc-TFPN[r)] COF (photoelectrocatalysis)	Solvothermal and post-modification strategy	N/A	Theoretical results demonstrated this catalyst has a low onset potential of -0.24 V, which is better than those of noble catalysts	118
Suzuki−Miyaura coupling reaction	Pd NPs@Thio-COF	Solvothermal and impregnation deposition	A Dimethylformamide/H_2O solution containing arylhalide, phenylboronic acid, K_2CO_3, and Pd NPs@Thio-COF are mixed in Schlenk tube	The coupling reaction of 1-iodine-4-toluene with phenylboric acid was catalyzed and the yield was > 99%.	65

[a)]FE: Faraday efficiency; [b)]MIS: Metal–insulator–semiconductor; [c)]TOF: Turnover frequency; [d)]TEOA: Triethanolamine; [e)]MeOH: Methanol; [f)]DCM: Dichloromethane; [g)]TpPa-1: Ketoamine-based COF; [h)]MeCN: Acetonitrile; [i)]Thio-COF: Thioether-containing COF; [j)]CCOF-MPC: Chiral COF carriers synthesized from cyanuric chloride and S-(+)-2-methylpiperazine; [k)]TON: Turnover number; [l)]TpTta: COF material constructed by 4,4′,4″-(1,3,5-Triazine-2,4,6-triyl)-trianiline (Tta) and 1,3,5-Triformyl phloroglucinol (TFP); [m)]NIS: N-iodosuccinimide; [n)]DMSO: Dimethyl sulfoxide; [o)]VASP: Vienna ab initio simulation package; [p)]S–COF: A 2D COF modified with thiol chains; [q)]EB-COF: Br is Br-functionalized COF. [r)]MO: Methyl orange; [r)]Pc-TFPN: Pc is 2,3,9,10,16,17,23,24-octahydroxyphthalocyaninato metal acronym, and TFPN is tetrauorophthalonitrile

713 acronym.

View Article Online
DOI: 10.1039/D1TA04439G

4.1 Photocatalytic reaction

Since the 1972s, Fujishima and Honda discovered the photocatalytic water splitting to produce H_2,[119] the expansion of photocatalytic systems and the study of photocatalytic mechanisms have become a hot spot in the field of catalysis. Using sunlight as a driving force to resolve the current environmental pollution crisis is a purpose that is fully in line with the "environmentally friendly" development strategy. In recent years, from inorganic semiconductors (TiO_2,[120] ZnO,[121] CdS,[122] $SrTiO_3$,[81], and MOF[123] etc.) to organic catalyst (g-C_3N_4,[124] etc.) and from homogeneous catalytic reaction to heterogeneous catalytic reaction, photocatalysis has drawn lots of attention. However, these photocatalysts have some disadvantages such as non-tunable structure, low light capture ability, and poor stability. COFs, as a "new star" in the catalysis industry, can well avoid these shortcomings and show their unique advantages in the photocatalytic reaction system: (1) the functional structure can be tuned through functional building blocks; (2) The covalent bond and π conjugation between the building units not only extend the life of the photoelectron but also ensure the stability of the catalytic system; (3) The permanent porous structure provides a huge specific surface area for catalytic reactions; (4) It can integrate photosensitizer and catalyst to promote the rapid development of photocatalytic system. These excellent properties have attracted scientists' attention and have led to rapid development in recent years. This section briefly introduces the application of COF-anchored NPs, NCs and single atom for photocatalysis.

4.1.1 Water splitting

View Article Online
DOI: 10.1039/D1TA04439G

Secondary energy is the link that connects primary energy. Hydrogen (H_2), as the cleanest and most abundant secondary energy source on earth, has attracted much attention of researchers for its production, storage, and transportation. At present, H_2 production by photocatalytic water splitting is one of the most potential method with the advantages of no secondary pollution, green, easy operation, and so on. However, the development of efficient and stable photocatalysts is fraught with challenges. Therefore, the research and development of photocatalysts is the key to the current development of this technology. Because the advantages of high specific surface area, high stability, high crystallinity, etc., COFs have shown great potential in realizing high-activity artificial photocatalytic systems.

As for photocatalytic water splitting to produce H_2, it is necessary to find a stable and efficient catalyst to promote proton reduction reaction. Besides, some catalysts require added photosensitizer (PS) in the catalytic system to broaden the photosensitive performance of the catalysts. Studies have found that the use of a molecular co-catalyst-COF system can produce considerable H_2 from solar energy without adding PS.[125] In this molecular co-catalyst photocatalytic system, COFs not only work as a support to anchor other active metal sites, but also use as PS to enhance the light absorption in the visible light region, thereby improving long-term H_2 evolution ability. The largest rate of H_2 produced by this system has increased by 17% compared with other photocatalytic systems.[126, 127] The microkinetic simulation of the reaction system shows that the transfer of outer-sphere electrons from light absorber to catalyst is the rate-limiting step. Thus, the COFs or COF-based materials using as the electron transfer and

View Article Online
DOI: 10.1039/D1TA04439G

light collector not only improves the efficiency of H_2 production, but also simplifies the experimental procedures.

By rationally selecting organic and inorganic semiconductors to construct photocatalytic water splitting system to produce H_2, the rate of H_2 production can be effectively increased. Due to its good photocatalytic performance, tunable structure, and high porosity, COF/CdS exhibited excellent performance in photocatalytic water splitting.[48] Studies have shown that the interfacial charge transfer between CdS and support played a crucial role in catalytic performance.[128] More importantly, the formed semiconductor heterojunction effectively promoted the separation of photogenerated carriers. Therefore, in this special semiconductor-semiconductor heterojunction, the strong interaction between two semiconductors promoted the rapid transfer of photogenerated electrons, thereby increasing the H_2 evolution reaction rate. The option excitation dynamics between COFs and CdS NPs could be more clearly felt through the H_2 evolution mechanism exploration (Fig. 7a). It was noted that a classic volcano curve of H_2 evolution rate was obtained with the increase of loading amount of CdS, by showing a first increase followed by a decrease. Furthermore, R. Banerjee and co-workers used COF as a substrate for dispersing CdS, which could control the growth of CdS NPs and provide a stable reaction environment.[102] And the stability tests of CdS, COF and CdS/COF were carried out for three consecutive cycles of 4 hours each. There was no deactivation of CdS/COF, while the stability of CdS and COF was poor. The use of COF as the carrier not only improves its own stability but also makes up for the shortcomings of CdS photo-corrosion.[129] It further highlights the excellent

View Article Online
DOI: 10.1039/D1TA04439G

characteristics of COF as a substrate and also explores the potential application of COFs as a sacrificial electron donor.

In the photocatalytic system, in addition to the above-mentioned semiconductor-semiconductor heterojunction, Schottky junction, another type of heterojunction, also can inhibit the recombination of photogenerated electrons-holes.[130] However, the traditional Schottky junction has disadvantages such as low efficiency and poor separation of charge carriers.[131] In order to further improve charge separation efficiency, Roeffaers et al. designed a metal-insulator semiconductor (MIS) photosystem based on COFs semiconductor.[93] It realized the efficient extraction of light-excited hot π-electrons in COFs, which were transferred to active metal sites (Pt NPs) through the ultra-thin PVP insulating layer, and the hydrogen evolution reaction (HER) performance had a great enhancement (Fig. 7b). It can be seen from the figure 7b that the carrier separation efficiency in COF-based MIS optical system is 32 times higher than that of the traditional MIS optical system. It is worth mentioning that the author's evaluation of the stability of this system is "Robust".

According to previous studies, the π conjugation of COFs possesses several advantages, which can decrease band gap, enhance photosensitivity, promote charge carrier generation, and accelerate carrier transport.[94, 132] Hence, the researchers used COFs with higher π conjugation to anchor CdS NPs (CdS-COF) for H_2 generation by water splitting.[102] Compared with pristine CdS and COFs, the photocatalytic activity of CdS-COF for H_2 generation has a substantial improvement. Because the π conjugation in carbon fiber promotes photoelectron stability, the interaction between π-π stacked

View Article Online
DOI: 10.1039/D1TA04439G

layered structure and CdS NPs can not only prevents the aggregation of CdS NPs, but also reduces the photo-corrosion of pure CdS (this phenomenon can be explained by the photoinduced annealing of the composites during photocatalysis, resulting in recrystallization at the conjugated polymer/inorganic nanocrystal interface.[133]). Therefore, the system shows higher activity and stability during the photocatalytic H_2 generation. To further highlight the advantages of π conjugation of COFs, Jiang and co-workers synthesized sp^2 carbon-conjugated COFs (sp^2c-COF) and loaded Pt NPs, and then evaluated the catalytic performance of Pt NPs@sp^2c-COF by photocatalytic decomposition of water for hydrogen production.[74] The author verified the following advantages of π conjugation of COF through experiments: First, The COF skeleton with C=C (sp^2 hybridization) covalent bond was very stable and could maintain the crystal structure for a long time. Second, the π conjugation of COF skeleton could generate narrow band gap (2.05 eV), thereby expanding the visible light absorption spectrum. Third, the π conjugation lattice can adjust the front track so that excitons could promote forward electron transfer in the π networks to prevent reverse charge recombination. Finally, π conjugation of COF has high porosity, which could supply more active sites for catalytic reaction. In the photocatalytic H_2 evolution system, sp^2c-COF played the role of collecting light, while π conjugation plays an important role in separating the light-generating carriers (Fig. 6). The Pt well confined in the pores of sp^2c-COF, as a cocatalyst, improves the hydrogen evolution efficiency. In addition, in most cases where COFs are used to anchor metal active sites, COFs need to link an N-rich functional group to make the metal active sites more stable on the carrier during the

View Article Online
DOI: 10.1039/D1TA04439G

water splitting process.[45] Scientists use nitrogen-rich COFs to anchor Pd/Pt NPs. Here the N is used as the junction to link COFs and metal NPs. This not only promotes the formation of smaller nanoparticles, but also accelerates the separation of photogenerated electrons and holes (Fig. 7c). Photoluminescence (PL) spectroscopy clearly displays that the material without Pd/Pt NPs shows a strong charge recombination rate. It further illustrates that the metal NPs can be anchored on COFs to form a tight interface, thereby accelerating the photoelectron transfer rate, and increasing the yield of hydrogen. In the water splitting reaction that converts solar energy into hydrogen energy, the use of COF-based materials to construct a reaction system has broad prospects.

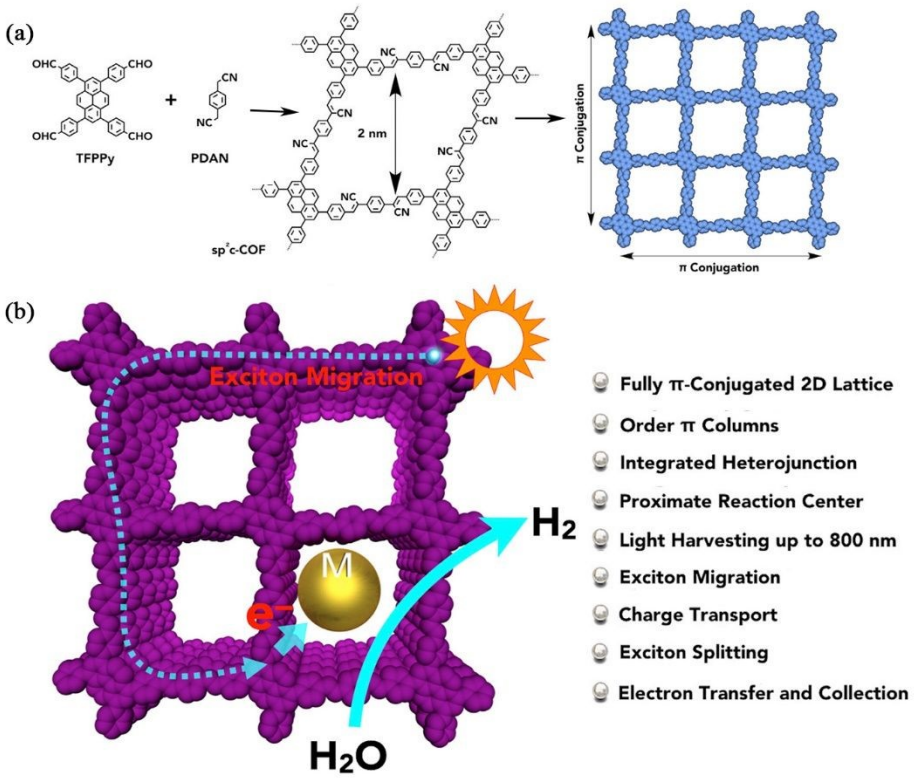

Fig. 6 (a) Schematic representation of the synthesis of the tetragonal sp^2c-COF by C=C bond polycondensation, and reconstructed crystalline 2D layer of sp^2c-COF that allows

View Article Online
DOI: 10.1039/D1TA04439G

the π conjugation along both the x and y directions (Reproduced with permission.[74] Copyright 2019, Elsevier); (b) Assembled light-driven interlocked system for hydrogen production from water based on a crystalline sp^2 carbon-conjugated framework and Pt water-reduction centers. The processes of photoenergy harvesting, electron transfer, and water-reduction reaction are seamlessly integrated in the system (Reproduced with permission.[74] Copyright 2019, Elsevier).

4.1.2 Carbon dioxide reduction reaction

As we know, CO_2 seriously endangers the living environment of human and animals. In order to mitigate this endangerment, reducing CO_2 in the atmosphere is one of the most challenging tasks facing all mankind.[134, 135] Under normal circumstances, CO_2 is very stable, and a lot of energy must be input to reduce it. [136, 137] Inspired by the "photosynthesis of plants", the use of photocatalysis to convert solar energy into the energy required for CO_2RR is currently one of the most economically feasible methods.[138] Photocatalytic reduction of CO_2 has been extensively studied using heterogeneous catalysts,[139] this is because photocatalytic system for CO_2 reduction is relatively stable, and the products can be easily separated. Unfortunately, the low catalytic activity limits its development. Therefore, finding high-activity catalysts has become an important goal for the development of heterogeneous reactions. Recently, the unique characteristics of COFs have been used as anchoring sites for metal species to participate in the heterogeneous reactions. In addition, COFs can not only selectively capture CO_2 gas, but also bind metal sites with high active, thereby creating a better reaction environment for CO_2 reduction.[140, 141] In this section, we review COFs-

View Article Online
DOI: 10.1039/D1TA04439G

confined catalysts in the CO_2 reduction reaction (CO_2RR).

Because COFs alone cannot fix the metal active sites well, some functional groups such as imine and pyridine are usually introduced during the synthesis of COFs. The N-rich sites of these groups can anchor the active site more stably. Chen et al. designed and synthesized a new N-rich COF-based material (FPy-COF) with metal coordination sites and had good adsorption performance for Co.[78] Studies showed that the newly synthesized catalyst materials not only improved the adsorption energy of CO_2, but also ensured the crystallinity of the materials. Fig. 7d showed that the recovered catalyst still maintained good photocatalytic activity during the reaction process. The DFT calculation further showed that FPy-COF provided a channel for metal coordination and charge transfer in the photocatalytic system for the reduction of CO_2 to CO. In 2016, Baeg and co-workers found that COFs could reduce CO_2 to formic acid (HCOOH) under solar light conditions,[142] but its selectivity and charge transfer rate were not ideal. Therefore, to improve the catalytic performance of COF-based materials, it is still a hot topic to find efficient and economical catalysts for CO_2 reduction.

Since metal centers can activate CO_2 molecules under light illumination condition, while most metal catalysts are prone to agglomeration and deactivation.[143] Therefore, the development of metal-functioned COFs is also a promising strategy to promote CO_2RR. Studies have found that ruthenium nanoparticles (Rh NPs) and COFs can build a heterogeneous catalytic system for CO_2RR, which can produce HCOOH with high efficiency (Fig. 7e).[116] For most semiconductor materials, the recombination of photo-generated carriers is an important factor affecting the photocatalytic efficiency. UV-

View Article Online
DOI: 10.1039/D1TA04439G

visible diffuse reflectance spectroscopy (DRS) and electrochemical impedance spectroscopy (EIS) displayed that the COF loaded Ru NPs not only improved charge transfer efficiency, but also enhanced absorption intensity of visible light. Only HCOOH products can be detected through gas and liquid phases, indicating that this catalytic system has high selectivity. In addition, the crystallinity and stability of composites in the cyclic reaction are also important bases for evaluating photocatalytic efficiency. Therefore, the author carried out five photocatalytic CO_2 reduction tests on the Ru NPs/COF, and finally characterized the reaction materials by XRD and Fourier transform infrared spectroscopy (FT-IR) to verify their high durability.

4.1.3 Organic pollutant degradation reaction

Although the research on supported catalysts is still in its infancy, it is an effective strategy to use COFs or COF-based materials as support nanomaterials to prepare COFs-confined catalysts for the degradation of pollutants.[144] Recently, wastewater containing organic dyes has attracted attention, because these organic dyes are complex aromatic compounds, posing a serious threat to public health and the environment.[10, 145] Therefore, photocatalytic technology is used to degrade organic dye wastewater, which has the advantages of simple operation and no secondary pollution. But in the conventional photocatalytic system, photo-generated electrons and holes are easily recombined,[146] Recently, researchers have proposed the Z-scheme system, which can avoid the above phenomenon, and the recombination rate of photogenerated electrons can be effectively reduced, and the rapid migration of photogenerated electrons can be promoted.[43] Du and co-workers anchored gold nanoclusters (Au NCs) on thiol-chain-

View Article Online
DOI: 10.1039/D1TA04439G

903 modified COFs to construct the Z-scheme system, and an Au-S-COF bond bridge was
904 formed (Fig. 7f). They found that this system showed excellent performance in the
905 degradation of pollutants (i.e., after 5 cycles, the removal rates of rhodamine B and
906 bisphenol A in water remained above 93.2% and 90%, respectively). Further, the time-
907 resolved photoluminescence emission decay spectra showed that the electron lifetime
908 was very long, which meant that the carrier separation efficiency was high, thereby
909 resulting in high performance for pollutant degradation. Unlike the traditional Z-
910 scheme system, this system did not have a potential difference in charge transfer
911 between energy levels, resulting in a higher redox capability.[147] The use of COF-based
912 materials to construct a new Z-scheme system has industrial value for the efficient
913 degradation of pollutants.

914 In recent years, lead halide perovskites have attracted extensive attention due to
915 their excellent optical properties.[148] But the toxicity of lead-based materials inhibits its
916 development. Using the porosity of COFs or COF-based materials to encapsulate
917 perovskite NCs ($CsPbBr_3/Cs_4PbBr_6$@EB-COF: Br) to reduce the environmental harm
918 of lead-based materials has been reported.[108] The photodegradation rate of MO (10 mL;
919 100 ppm) by $CsPbBr_3/Cs_4PbBr_6$@EB-COF: the Br catalyst driven by visible light is
920 0.245 min^{-1}. In the cycle test, this catalyst showed excellent stability. Unfortunately,
921 $CsPbBr_3/Cs_4PbBr_6$ NCs aggregation occurred in the cycle experiment, and the author
922 did not indicate whether the aggregated material was leached or not. It is an important
923 topic that need to be solved at present when using the catalyst with good photocatalytic
924 performance but containing toxic substances to treat actual water.

View Article Online
DOI: 10.1039/D1TA04439G

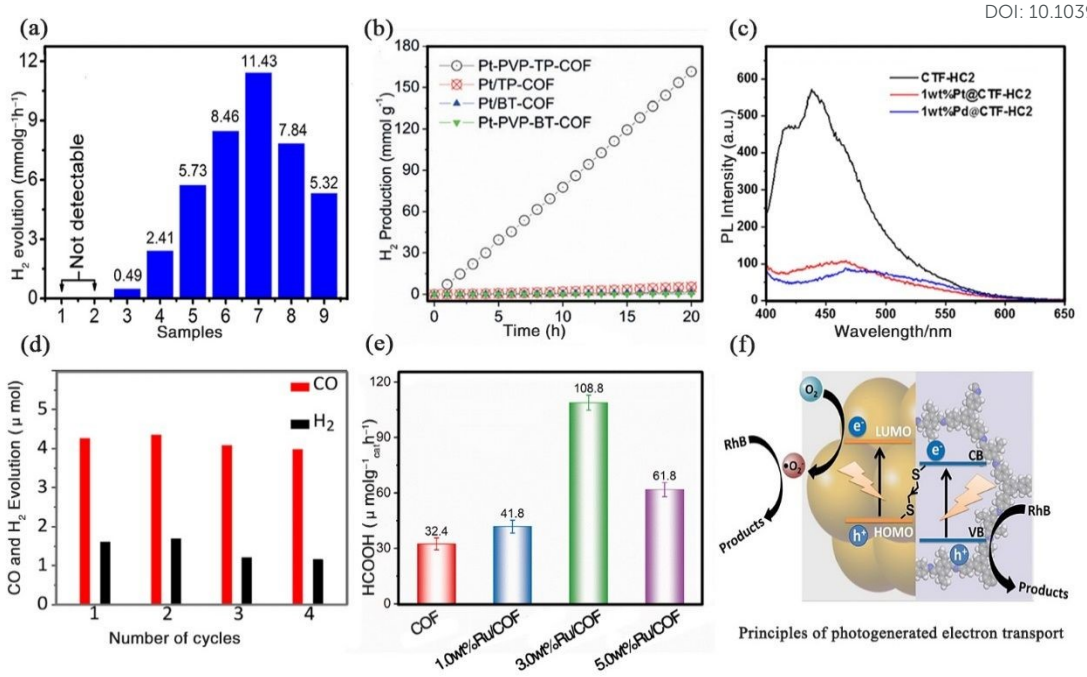

Fig. 7 (a) (Color online) The amount of hydrogen evolved over 1, no catalyst, 2, without light irradiation, 3, COF, 4, CdS, 5, 5%CdS-COF, 6, 10%CdS-COF, 7, 20%CdS-COF, 8, 40%CdS-COF and 9, 20%CdS-COF (Reproduced with permission.[48] Copyright 2020, Elsevier); (b) Photocatalytic hydrogen evolution under visible light irradiation in the presence of ascorbic acid (Reproduced with permission.[93] Copyright 2019, Wiley Online Library); (c) Photoluminescence (PL) spectroscopy for COFs, 1wt% Pt@COF and Pd@CPF (Reproduced with permission.[45] Copyright 2020, ACS Publications); (d) CO and H_2 production by Co-FPy-CON over multiple 2 h repeat runs. The sample was degassed, and 1 μmol of $(Ir[dF(CF_3)ppy]_2(dtbpy))PF_6$ was added after each run. (Reproduced with permission.[78] Copyright 2020, ACS Publications); (e) Amount of the produced HCOOH over the prepared catalysts upon 10 h of visible-light irradiation (800 nm ≥ λ ≥ 420 nm). Photocatalyst: 15 mg, MeCN/TEOA volume ratio: 10/1, and total solution volume: 110 mL (Reproduced with permission.[116] Copyright 2021,

View Article Online
DOI: 10.1039/D1TA04439G

Elsevier); (f) Principles of photogenerated electron transport between Au NCs and the COFs support (e@ in LUMO and h^+ in HOMO represent a photogenerated electron and hole of Au NCs, respectively; e@ in CB and h^+ in VB represent a photogenerated electron and hole of COF-V, respectively) (Reproduced with permission.[43] Copyright 2020, Wiley Online Library).

4.2 Electrocatalytic reaction

In electrocatalysis, an electrocatalyst with a lower overpotential is usually prepared to reduce voltage loss and improve electrocatalytic efficiency. The research shows that COF-based electrocatalysts not only show a low overpotential,[149] but also exhibit good selectivity and durability in electrocatalysis. Hence, in this section, we will focus on summarizing the applications of nanoparticles, nanoclusters, and single atom embedded COFs or COFs-based materials in electrocatalysis. COFs-confined catalysts in the field of electrocatalysis have the advantages of controllable reaction rate and high selectivity, which has promoted the development of HER,[150] ORR,[151] OER,[152] CO_2RR,[153] etc.

4.2.1 Hydrogen evolution reaction

Hydrogen plays an important role in many industrial productions and has excellent properties such as renewable, zero pollution, and high calorific value. At present, platinum (Pt) based material for HER is considered to be the most efficient catalyst.[154] The high-performance Pt-based electrocatalysts for the HER are usually determined by their intrinsic activity and the stability of supporting materials. Recently, COFs with bipyridine groups has shown excellent metal-chelating abilities,[96] and ultra-high porosity and stability, which realizes the high dispersion and low leaching rate of ultra-

View Article Online
DOI: 10.1039/D1TA04439G

fine metal NPs and effectively improve the electrocatalytic reaction rate. The outstanding performance of COF-based materials is ascribed to the fact that COF has a strong interaction with Pt NPs (PtNPs-@COF) and Pt NPs do not agglomerate, making this catalyst superior to Pt/C in an alkaline environment. The electrocatalytic performance of PtNPs @COF (0.071 mg on carbon paper, 6.09 wt. % Pt) for hydrogen production is 13 times larger than that of Pt/C (0.071 mg on carbon paper, 10 wt. % Pt) (Fig. 8a). The TEM images showed that the structure of the catalyst did not change after reuse for 5 times. Therefore, the catalyst had high stability and resistance to degradation in aqueous solution. In this study, the authors incorporated nanoparticles into COF pores, which provided more metal active centers, thereby improving electrocatalytic reaction rate.

4.2.2 Carbon dioxide reduction reaction

Using electrocatalysis technology to reduce carbon dioxide and convert it into high value-added chemical products or fuel is an effective way to realize chemical energy storage.[155] In order to reduce carbon dioxide efficiently and stably, Zheng and co-workers proposed a two-step electrocatalytic reaction system by imitating the two-step mechanism of "light reaction + carbon reaction" in green plant photosynthesis (Fig. 8b), which could efficiently reduce CO_2 to CO.[156]

Although the efficiency of CO_2 reduction and fixation in the above system was satisfactory, it was necessary to effectively solve the problem of the low solubility of CO_2 in water to realize large-scale utilization of CO_2.[156] To solve this problem, researchers have tried a lot and a strategy is developed, namely, CO_2 is introduced into

View Article Online
DOI: 10.1039/D1TA04439G

the reduction center of the electrocatalytic material, thereby reducing the escape of CO_2 from the electrolyte.[157] A new type of cobalt-functioned COF-based materials is used to realize the integration of CO_2 storage and CO_2 reduction. The concentration of CO_2 in this new material is 97.7 times higher than the concentration of CO_2 in the water through the reasonable design and DFT calculations, which not only lowers the reduction barrier (i.e., the overpotential decreased from 0.39 to 0.27V), but also increases the yield of CO (i.e., the reaction rate increased by 97.7 times). Therefore, integrating the storage unit into the electrode can effectively improve the efficiency.

In the CO_2RR, the surface of electrocatalyst is prone to self-reconstruction.[158] This self-reconstruction will make it difficult to identify the active center and easy to get error phenomenon analysis. In this context, operando X-ray adsorption fine structure analysis was found,[71] this analytical method can accurately determine the location of the active site and reveal the point-driven dynamics. Therefore, the operando identification of the activity center and the unique constraint behavior of the COFs provide valuable insights for further research on the structure-performance relationship.

4.2.3 Oxygen reduction reaction

ORR is an important reaction in metal-air batteries and multi-type combustion batteries, which can determine energy conversion efficiency and power density.[159-161] At present, only Pt-based materials are used as actual ORR catalysts, but the development of Pt-based ORR catalysts has some problems such as low reserve, high costs, and poor stability, which is not suitable for commercialization.[162, 163] Therefore, the development of ORR catalysts with earth abundance, good stability and high

View Article Online
DOI: 10.1039/D1TA04439G

performance is essential to promote its development.

According to previous studies, it is feasible to use transition metal-containing materials to replace Pt-based materials in ORR, because the d orbitals of transition metal elements are empty, and it is easy to form complexes. Based on the Sabatier principle, when measuring the activity of ORR on different metal surfaces, the volcanic trend of ORR activity and the strength of absorbed oxygen is obtained (Fig. 8c).[112, 164]The ORR activity of the metal surface at the top of the volcanic graph is the highest. This principle shows that there is a suitable interaction between ORR catalyst and main intermediate. Thus, the development of ORR catalyst requires precise adjustment of the adsorption energy of the intermediate.[77] By selecting appropriate transition state metal atoms (Mn, Fe, Co, Ni, and Cu) doped in COFs and/or coordination numbers (CN) as parameters, the adsorption strength is adjusted near the volcano peak, thereby improving the catalytic activity. First-principles calculations show that the greater the number of d-electrons of the transition metal atoms and the closer the d-band center is to the Fermi level, the stronger the binding energy of the resulting reaction intermediate to the surface. For metal atoms with smaller CN, ORR intermediates have a strong adsorption effect. According to the correlation between the adsorption strength of the catalyst to ORR and the number of active sites, while changing the number of d-electrons and CN, an ORR catalyst with higher activity and stability can be obtained. Transition metal atoms have attracted much attention because of their unique d-band center, which can distinguish the changing trend of the interaction energy between different metal surface adsorbates and metals. COFs and COF-based materials acted as

View Article Online
DOI: 10.1039/D1TA04439G

a carrier of transition metal atoms in this system, providing a good reaction environment, which not only prevented the aggregation of metal atoms, but also prevented metal atoms from being corroded by solvents. This is useful for rational design and construction of highly active and stable ORR, and also laying the cornerstone for the precise design of COF-confined materials.

Although first principles have proven that COFs or COF-based materials can firmly anchor transition metal (TM) atoms during synthesis and catalysis, few studies have shown the interaction mechanism between TM atoms and organic ligand. Recently, some researchers have elaborated on the role of the p-electrons of carbon atoms and the d orbitals of TM atoms by describing the catalytic activity of ORR.[79] Through Bader analysis, a promising method is provided to adjust the adsorption strength of TM atoms and intermediate products. These studies have shown that the best position for adsorption is on the C atom adjacent to the N atom for TM atoms. Because the p-band center of bone C atom is beneficial to the adsorption of Tm atoms and the transfer of electrons, it can be used to describe and optimize the catalytic activity of ORR. In addition, the π−π conjugation in COFs also helps to improve the electron transport in the reaction. And the p-d hybridization formed by the p-electrons of the C atoms and the inherent d-orbital of the net charge of the TM atoms also can provide additional degrees of freedom to adjust the catalytic performance of ORR. Based on above-mentioned analysis about COFs-anchored TM atoms, we found that this catalyst possessed excellent performance (i.e., Cr-, Mn-, Co-COFs the overpotential are 0.29, 0.31, and 0.24 V), which was comparable to the most famous noble metal catalysts

View Article Online
DOI: 10.1039/D1TA04439G

(Pt/C). This study not only provided a new family for high-efficiency ORR, but also illustrated the excellent quality of COFs-confined catalysts through first principles calculations, thereby laying a new foundation for the development of COFs-confined catalysts. This will not only increase the cost of the electrocatalytic system, but also leads to the complexity of designing experiments. Whereas it is necessary to find an electrocatalytic system that is in line with the development of practical applications to effectively avoid the above phenomenon.

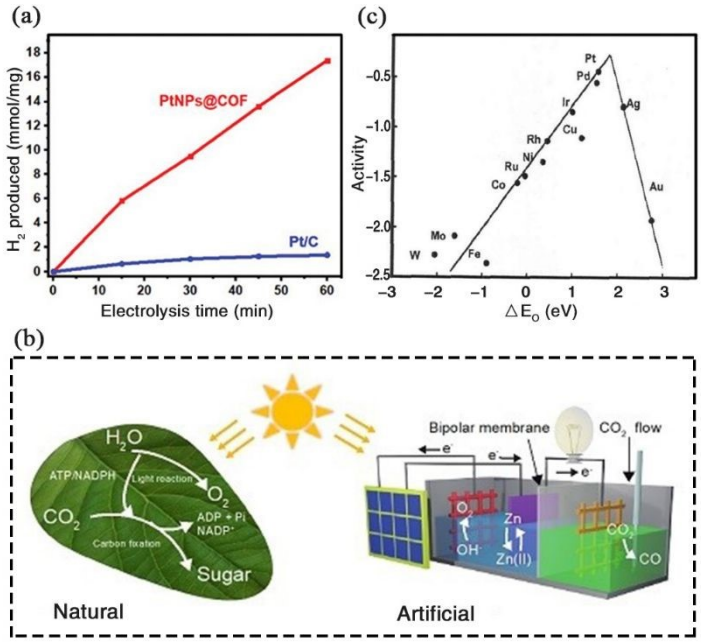

Fig. 8 (a) The amount of hydrogen evolution by PtNPs@COF (red rectangular) and Pt/C (blue circle) (Reproduced with permission.[48] Copyright 2020, Elsevier); (b) Schematic diagram of a new carbon dioxide electrochemical reduction system (Reproduced with permission.[156] Copyright 2018, Nature); (c) The relationship between oxygen reduction activity trend and O binding energy (Reproduced with permission.[164] Copyright 2004, ACS Publications).

4.3 Other reactions

View Article Online
DOI: 10.1039/D1TA04439G

4.3.1 Reduction of 4-nitrophenol

At room temperature, the use of sodium borohydride ($NaBH_4$) for reducing 4-nitrophenol (4-NP) to 4-aminophenol (4-AP) has high chemical significance.[165] This is because reducing highly toxic 4-NP to low-toxic 4-AP not only reduces the harm of 4-NP for the natural environment, but also generates high-value 4-AP, which is important intermediates to synthesize a variety of fine organic chemical materials. [166]

Metal NPs have attracted much attention because of their excellent catalytic performance. Among them, Au NPs hold ultra-high surface energy and become the most potential catalyst for the catalysis industry.[167] However, the Au NPs are easy to agglomerate without suitable support during the catalytic process, resulting in reduced catalytic performance. Zhu's groups reported an encapsulation technology that Au NPs were confined in COFs to prevent their leach and improve stability.[61] The pseudo-first-order kinetics of COF-based composite containing 0.2 wt. % of 15 nm Au NPs is the strongest. All 4-NP were reduced within 10 min, and the reduction product was just 4-AP. However, the reactivity of this material wound decrease as the number of cycles increases, XRD and TEM showed that the microstructures and crystallinity of COFs composite material were maintained. Therefore, author concluded that the reduction in reaction activity may be due to the loss of catalyst during the cycle washing process. In general, this simple and flexible encapsulation technology promotes the development of heterogeneous catalyst preparation. However, the successful development of stable and highly active catalysts was still the mainstream of heterogeneous catalysis. Recently, Ding's group used sulfur bonds to connect COFs and Au NPs in Au-S-COF,[59]

View Article Online
DOI: 10.1039/D1TA04439G

which showed excellent catalytic performance in 4-NP reduction (Fig. 9a). The whole 4-NPs were reduced to 4-AP within 7 min. After ten cycles of reactions, the catalytic efficiency still remained above 90%, and the structure and morphology did not have obvious changes, indicating that the catalyst had high stability and recyclability. It was because that the sulfur bond in the COFs could well strengthen the interaction between the nanoparticles and the COFs. By using COFs to form a special pore structure to anchor metal NPs for 4-NP reduction, it promotes the progress of COFs-confined catalysts in heterogeneous catalytic reactions.

Li and co-workers used the first encapsulation etching technology to embed palladium nanoparticles (Pd NPs) in COFs.[62] The active site was exposed by etching the encapsulation materials, and the yolk-shell nanostructure was formed, which had a chemical significance for the reduction of 4-NP. The formation of internal voids enhanced mass transfer and expanded adsorption range, leading to increased catalytic efficiency (4-NP was completely converted to 4-AP within 8 min). The first-order reaction kinetics rate constant was 0.41 min^{-1}, further illustrating its high catalytic activity. Meanwhile, there was no obvious loss of catalytic activity after many repeated operations, confirming its high recyclability. However, the catalytic activity was affected by the thickness of COFs shell, and the reaction rate decreased as the thickness increased. Studies showed that anchoring platinum nanoparticles (Pt NPs) on COFs containing sulfide functional groups could well inhibit this phenomenon.[62] And this catalyst exhibited outstanding catalytic activity in reducing 4-NP (Fig. 9b). Because the Pt NPs were anchored on the COFs to form an ultra-fine nanometer size, it only

View Article Online
DOI: 10.1039/D1TA04439G

took 8 min to reduce 4-NP due to the mesoporous structure of the COFs, and after 4 cycles, the morphological structure and catalytic activity did not change obviously, which highlighted the high crystallinity and stability of the catalyst. The rate constant reflected the catalytic activity of reducing 4-NP.[168] The calculations showed that first-order reaction kinetics constant increased as the size of metal NPs decreased.[169] Therefore, it is feasible to obtain NPs with smaller size to improve the catalytic activity, and COF's crystalline porous network and tunable building blocks[170] are important factors for the design and synthesis of ultrafine NPs.

4.3.2 Hydrogenation reaction

The selective hydrogenation reactions rate is related to the nanometer size of the metal absorbed on the support.[171] The research results show that the interaction between metal and support affects the activity of the hydrogenation reaction. Optimizing the COFs structure to anchor finer Pd NPs can obtain high activity.[50] When the average size of Pd NPs reaches 2.2 nm, which not only can generate more active sites, but also enhance the interaction between Pd NPs and COFs, thereby increasing the rate of hydrogenation reaction. In 2021, Yang and co-workers selected imine-linked COF with high specific surface area as the support for Pd NPs to form Pd NPs with a size of 1.8 nm.[72] The XPS analysis showed that the imine bond could control the growth of Pd NPs in the catalytic system and build charge transfer bridge with Pd NPs. Therefore, the catalytic performance of Pd NPs/COF catalyst in nitrobenzene hydrogenation reaction is much higher than that of commercial Pd/C (TOF: 906 h^{-1} vs. 507 h^{-1}). Therefore, optimizing COFs to control the size of metal species has important practical

View Article Online
DOI: 10.1039/D1TA04439G

significance for realizing high-efficiency hydrogenation reaction.

4.3.3 Organic reaction

H_2, as the gas with the smallest density and relative molecular mass known in the world, has led to its diversification.[172] Because H_2 is widely used in industries, fuels, medicine, etc., the production of H_2 has become a hot topic in the scientific community. When using $NaBH_4$ to produce H_2, water flooding is usually used to monitor the amount of the released H_2, and the use of COF-based (Co@COF) materials has been reported, and these catalysts displayed excellent performance in hydrogen generation.[67] The cyclic voltammogram (CV) revealed that Co@COF had relatively faster redox kinetics. This is due to the mesoporous structure and high crystallinity of COFs, which enhanced the electrons transportation. Meanwhile, Co NPs could grow in the pores of COFs to avoid the leach of Co NPs.

In green organic synthesis, it is a challenging method to selectively oxidate alcohols by molecular oxygen. The Pd NCs confined in optimized COFs have high activity for this reaction (Fig. 9c).[70] The kinetic shows that the conversion rate of benzyl alcohol is 97% after 32 h ($2C_6H_5CH_2OH + O_2 = 2C_6H_5CHO + 2H_2O$).[173] As expected, the metal particles with different sizes can be achieved by choosing different COFs building blocks. Therefore, it is not difficult to generate ultra-fine Pd NPs in COFs,[42] R. Banerjee and co-workers prepared COFs-confined catalysts (Pd NPs@COF) with high catalytic performance for 2-substituted benzofurans synthesis (Fig. 9d). Meanwhile, the prepared Pd NPs@COF showed high reproducibility and excellent stability in cycle test, proving its strong practicability. This work proposes a strategy for efficient synthesis of organics

View Article Online
DOI: 10.1039/D1TA04439G

and demonstrates that suitable COF building blocks can potentially control the growth of NPs. Based on these theoretical supports, Ma et al. selected the COF building block containing nitrogen atoms to confine Rh NPs,[68] and using ammonia as nitrogen source and hydrogen as hydrogen source to catalytic synthesis of secondary imine. Surprisingly, Pd NPs@COF showed universality and recyclability in the conversion of aromatic aldehydes to secondary imine. This greatly encouraged the researchers to further explore the universality of COFs-confined catalysts in heterogeneous catalysts.

Using heterogeneous catalysts to catalyze the synthesis of imine products, the corresponding catalytic selectivity is related to the morphology and structure of the support. The COFs with excellent performance have high catalytic selectivity for the one-pot synthesis of benzyl alcohol and amine after anchoring Ru NPs.[69] In addition, using different COFs or COF-based materials as supports are employed to combine coordination metals with linkers to improve the efficiency of heterogeneous catalytic reactions. They are also used in the hydroformylation reaction of 1-octene. The modification of COFs can not only stabilize the metal sites more effectively and increase the reaction space between reactants and active sites, but also improve the catalyst cycle life, thereby further expanding the scope of organic reactions.

View Article Online
DOI: 10.1039/D1TA04439G

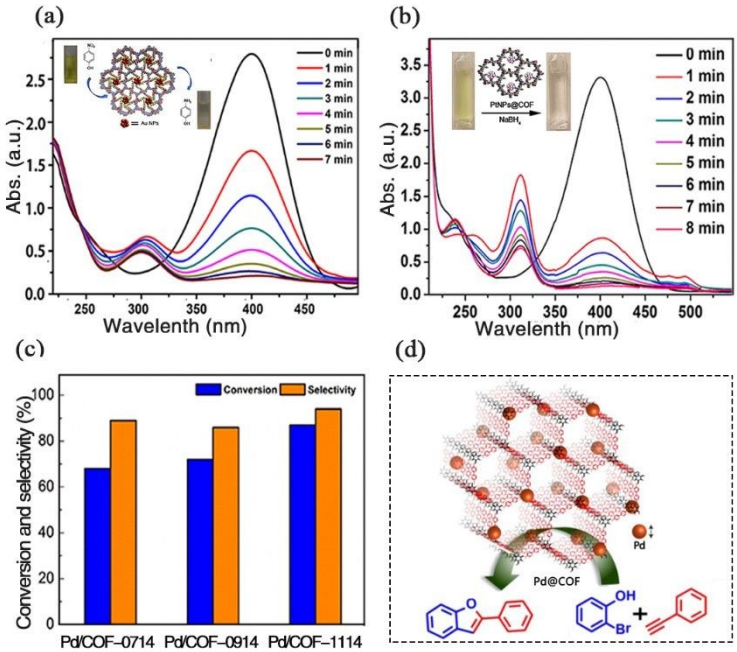

Fig. 9 (a) The UV–vis image of the reduction of 4-nitrophenol in the presence of Au-S-COF (Reproduced with permission.[59] Copyright 2017, Science); (b) Time-dependent UV−vis spectra of the reduction of 4-nitrophenol (0.3 μmol) catalyzed by 50 μL unsupported Pt NPs (0.17 mg mL^{-1}) (Reproduced with permission.[62] Copyright 2019, Wiley Online Library); (c) Catalytic performance of Pd/COF-300-xy series (xy = 0714, 0914, and 1114) in the benzyl alcohol oxidation reaction (Reproduced with permission.[70] Copyright 2020, ACS Publications); (d) Pd@COF catalyzes the synthesis of 2-substituted benzofurans from 2-bromophenols and terminal alkynes (Reproduced with permission.[42] Copyright 2017, ACS Publications).

5. Conclusion and prospect

The vigorous development of heterogeneous catalysts has supplied new opportunity to solve environmental pollution and other problems. These catalysts topography and reaction mechanisms are also diverse. In terms of supported catalysts, the related behavior of substances in the confined space (the confined space formed by

View Article Online
DOI: 10.1039/D1TA04439G

nano-particles and confined channel) and related chemical pathways will affect the environmental purification behavior and mechanism of catalysts. For most of the special supported catalysts zeolites-confined catalysts, MOFs-confined catalysts, and COFs-confined catalysts, the confined space of these catalysts can form a coordination complex with a single atom or multiple atoms. Therefore, the chemical state and coordination environment of the nano-particles that confined in the porous material may be different from original catalyst. At present, the information of limited three-dimensional structure limits us to better understand the relationship between the catalyst structure-reaction. Due to the low stability of MOFs-confined catalysts and the narrow reaction range of zeolites-confined catalysts,[11,174] the excellent performance of COFs-confined catalysts processes more practical for the future development of catalysis.

In this review, based on the structure-reaction relationship of the nano-particles with different sizes supported by COFs, the interaction between nano-scale particles and supported was re-recognized. In this way, we have a deep understanding of the growth process and structural characteristics of functional nano-scale particles in space. This way also can analyze the reaction behavior and mechanism of COFS limited catalyst in heterogeneous reaction. But the current academics' attention and research in this direction have just begun. In the design of the structure and performance of COF-confined catalysts, the study of the dynamic characteristics of between the active site and the reactant or the solvent, and the actual situation of their in environmental applications are far from enough. According to the interaction between nano-scale particles and supports, we further outline the influence of confinement effects on

View Article Online
DOI: 10.1039/D1TA04439G

heterogeneous catalytic systems: establish a close cooperative relationship (that is, carrier-based migration) between support and particle to increase the carrier transfer rate; the interaction between the confined space and the active site can optimize structure and maximize energy utilization. Therefore, a series of heterogeneous catalytic reactions were proposed to verify the catalytic efficiency of COFs-confined catalysts, such as organic pollutant degradation reactions, water splitting, CO_2RR, HER, ORR, reduction of 4-NP, hydrogenation reaction, and organic reaction.

Although the confinement effect plays a huge role in the heterogeneous catalytic system, it is difficult to realize the precise design of COFs-confined catalyst functioned with existing methods, and the relationship between the confinement effect and the catalytic system has not yet been clarified. Thus, COFs-confined catalysts are of great significance to future heterogeneous catalytic reactions compared to other catalysts, but there are still many challenges to overcome:

(1) For the morphology and structure of COFs-confined catalysts. The morphology and structure of the catalyst determine its performance. The morphology and structure of COFs or COF-based materials can be adjusted by selecting different building blocks to better prevent the agglomeration and deactivation. In addition, nano-scale particles have a strong interaction with COFs or COF-based materials, which increases the stability and continuity of the catalytic system. If we have a deeper understanding of the mechanism of this interaction on the adjustment of the supported catalyst's structure, we can adjust supports blocks according to the growth status and position of the anchored active site to optimize the morphology and structure of the COFs-confined

View Article Online
DOI: 10.1039/D1TA04439G

catalysts. Herein, based on the purposeful synthesis of zeolite materials by Li et al.,[175] we put forward a bold idea. Although it is not possible to have a deeper understanding of the internal interactions of the catalyst materials, we can purposefully design the structure of the active site according to the excessive state of the target reaction. Since the transition state of the heterogeneous catalytic reactions can describe the coordination complex of the active site in the COFs-confined catalysts, which is beneficial to our research on the structure of the COFs-confined catalysts active site.

(2) For the size effect of nano-sized particles (from nanoparticle to single atoms). In this article, most of N and S bonds are combined with metal to form a strong interaction N/S-metal bond. Although the metal active site can be fixed well, its growth size cannot be effectively controlled. Therefore, a large number of other technologies have appeared to limit the size effect of optimized particles, but the current improvement is not obvious, and it is difficult to control the growing of particles. This may be due to the fact that when nano-sized particles overcome the geometric limitations of COFs or COF-based materials support, which makes it difficult to control the growth process of the particles. In addition, the adjacent active sites in the pores of COFs or COF-based materials can work together to activate reaction.

(3) For the separation efficiency for carriers. Due to the tunability of COFs or COF-based materials, it can be given dual functions, such as the support and electron donor or carrier and heterogeneous photosensitizer, etc., to improve the separation efficiency of carriers. The separation efficiency of carriers also can be effectively improved by forming bond bridges, heterojunctions, Z-scheme systems, etc. between

View Article Online
DOI: 10.1039/D1TA04439G

nano-scale particles and carriers. It is worth noting that the intercalation of transition metals can accelerate the reaction kinetics and promote the separation of electron-hole pairs at the photoelectrode interface, but it is of little value in practical applications. What's more, we can accurately analyze the separation ability of carriers by calculating the relationship between the carrier concentration and the energy of the carriers and the relationship between the catalyst's own parameters. However, the calculation process is complicated, and many uncertain factors will lead to large errors, which cause difficulties in studying the carrier separation mechanism in depth. Therefore, this work is still important for the development of catalysts.

(4) For the methods of theoretical calculations and molecular simulation of COF-confined catalysts. The results of theoretical calculation of the relevant parameters for the modeling of the active sites in the COF-confined catalysts have large errors, which may lead to the misunderstanding of the structure of the COF-confined catalysts and the inconsistency between the reaction mechanism and reality. However, if theoretical design and modeling are carried out based on experiments to further demonstrate the reaction mechanism and material properties, it not only can effectively explain the experimental phenomenon, but also provide some parameter data for future development. These established models are static catalytic models rather than dynamic models. Therefore, the interaction between active site and reactants or solvents cannot be reasonably explained.

(5) For the application of COF-confined catalysts in the environment, it has shown excellent performance. We can verify the catalytic activity through different

View Article Online
DOI: 10.1039/D1TA04439G

heterogeneous catalytic reactions. At the same time, it also shows broad applications of this material, especially in environmental remediation and energy utilization, and the heterogeneous catalyst prepared by the strategy of embedding nano-particles into COFs or COF-based materials is committed to solving environmental problems and facing many urgent problems. For example, cost issues, performance issues, application single issues, and environmental risk issues.

Overall, COFs-confined catalysts exhibit abnormal thermodynamics, kinetics, and hydrodynamic properties and behaviors, which can achieve the chemical conversion and selectivity of pollutants under milder conditions. Although there is not much research on COFs-confined catalysts at present, many researchers have paid attention to the structure-reaction relationship of such supported catalysts. We believe COFs-confined catalyst will play a huge role in heterogeneous catalytic reactions in the future.

Acknowledgments

This study was financially supported by the Program for the National Natural Science Foundation of China (51779090, 51879101, 51579098, 51709101, 51521006, 51809090, 51909084), the National Program for Support of Top–Notch Young Professionals of China (2014), the Program for Changjiang Scholars and Innovative Research Team in University (IRT-13R17), Hunan Natural Science Foundation (2020JJ3009), Hunan Researcher Award Program (2020RC3025), Hunan Provincial Science and Technology Plan Project (2018SK20410, 2017SK2243, 2016RS3026), and the Fundamental Research Funds for the Central Universities (531119200086, 531118010114, 531118040083,541109060031).

View Article Online
DOI: 10.1039/D1TA04439G

Reference:

1. F. Society, *Science*, 1983, **193**, 19-22.

2. Q. Fu, F. Yang and X. Bao, *Accounts Chem. Res.*, 2013, **46**, 1692-1701.

3. A. Wang, J. Li and T. Zhang, *Nat. Rev. Chem.*, 2018, **2**, 65-81.

4. L. Liu and A. Corma, *Chem. Rev.*, 2018, **118**, 4981-5079.

5. M. Boudart, *Adv. Catal.*, 1969, **20**, 153-166.

6. L. Shang, Y. Liang, M. Li, G. I. N. Waterhouse, P. Tang, D. Ma, L.-Z. Wu, C.-H. Tung and T. Zhang, *Adv. Funct. Mate.*, 2017, **27**, 1606215.

7. Y. Zhu, Q. Lin, Y. Zhong, H. A. Tahini, Z. Shao and H. Wang, *Energy Environ. Sci.*, 2020, **13**, 3361-3392.

8. G. Eva María, P. M Teresa, P. Cecilia, L.-E. Alejandro, B. Mercedes, M. Manuel, C. Avelino, *Science*, 2017, **355**, 1051-1054.

9. Y. Hu, H. Zhang, P. Wu, H. Zhang, B. Zhou and C. Cai, *Phys. Chem. Chem. Phys.*, 2011, **13**, 4083-4094.

10. T. Zhang, G. Xing, W. Chen and L. Chen, *Mater. Chem. Front.*, 2020, **4**, 332-353.

11. L. Liu and A. Corma, *Nat. Rev. Mater.*, 2021, **6**, 244–263.

12. W. Zhou, Q. Y. Lin, J. A. Mason, V. P. Dravid and C. A. Mirkin, *Small*, 2018, **14**, e1802742.

13. B. C. Gates, M. Flytzani-Stephanopoulos, D. A. Dixon and A. Katz, *Catal. Sci. Technol.*, 2017, **7**, 4259-4275.

14. P. J. Waller, F. Gandara and O. M. Yaghi, *Acc. Chem. Res.*, 2015, **48**, 3053-

View Article Online
DOI: 10.1039/D1TA04439G

3063.

15. K. Chen, L. Yang, Z. Wu, C. Chen, J. Jiang and G. Zhang, *Phys. Chem. Chem. Phys.*, 2019, **21**, 546-553.

16. Z. Xiang, D. Cao and L. Dai, *Polym. Chem.*, 2015, **6**, 1896-1911.

17. X. Liu, D. Huang, C. Lai, G. Zeng, L. Qin, H. Wang, H. Yi, B. Li, S. Liu, M. Zhang, R. Deng, Y. Fu, L. Li, W. Xue and S. Chen, *Chem. Soc. Rev.*, 2019, **48**, 5266-5302.

18. T. Ma, L. Wei, L. Liang, S. Yin, L. Xu, J. Niu, H. Xue, X. Wang, J. Sun, Y.-B. Zhang and W. Wang, *Nat. Commun.*, 2020, **11**, 6128.

19. C. Gropp, T. Ma, N. Hanikel and O. M. Yaghi, *Science*, 2020, **370**, eabd6406.

20. C. Zhao, C. S. Diercks, C. Zhu, N. Hanikel, X. Pei and O. M. Yaghi, *J. Am. Chem. Soc.*, 2018, **140**, 16438-16441.

21. L. K. Wang, J. J. Zhou, Y. B. Lan, S. Y. Ding, W. Yu and W. Wang, *Angew. Chem. Int. Ed.*, 2019, **58**, 9443-9447.

22. J. Li, X. Jing, Q. Li, S. Li, X. Gao, X. Feng and B. Wang, *Chem. Soc. Rev.*, 2020, **49**, 3565-3604.

23. R. K. Sharma, P. Yadav, M. Yadav, R. Gupta, P. Rana, A. Srivastava, R. Zbořil, R. S. Varma, M. Antonietti and M. B. Gawande, *Mater. Horiz.*, 2020, **7**, 411-454.

24. L. Guo and S. Jin, *ChemPhotoChem*, 2019, **3**, 973-983.

25. S. Cao, B. Li, R. Zhu and H. Pang, *Chem. Eng. J.*, 2019, **355**, 602-623.

26. H. Hu, Q. Yan, R. Ge and Y. Gao, *Chinese J. Catal.*, 2018, **39**, 1167-1179.

View Article Online
DOI: 10.1039/D1TA04439G

27. J. Guo and D. Jiang, *ACS Cent. Sci.*, 2020, **6**, 869-879.

28. J. Liu, N. Wang and L. Ma, *Chem. Asian. J.*, 2020, **15**, 338-351.

29. H. Wang, H. Wang, Z. Wang, L. Tang, G. Zeng, P. Xu, M. Chen, T. Xiong, C. Zhou, X. Li, D. Huang, Y. Zhu, Z. Wang and J. Tang, *Chem. Soc. Rev.*, 2020, **49**, 4135-4165.

30. M. Haruta, N. Yamada, T. Kobayashi and S. Iijima, *J. Catal.*, 1989, **115**, 301-309.

31. M. Valden, X. Lai and D. W. Goodman, *Science*, 1998, **281**, 1647-1650.

32. Gates and C. B., *Chem. Rev.*, 1995, **26**, 511-522.

33. J. R. Cabrero-Antonino, R. Adam, V. Papa and M. Beller, *Nat. Commun.*, 2020, **11**, 3893.

34. S. Mitchell, E. Vorobyeva and J. Perez-Ramirez, *Angew. Chem. Int. Ed.*, 2018, **57**, 15316-15329.

35. G. S. Parkinson, *Catal. Lett.*, 2019, **149**, 1137-1146.

36. H. Yang, L. Jin-Cheng, L. Langli, W. Yang-Gang, Z. Junfa, D. Yingge, L. Jun, S. X. Mao and W. Chongmin, *Proc. Natl. Acad. Sci. U. S. A.*, 2018, **115**, 7700.

37. C. H. M. a. K. P. d. J. Tom W. van Deelen, *Nat. Catal.*, 2019, **2**, 955-970.

38. C. Y. Lin, D. Zhang, Z. Zhao and Z. Xia, *Adv. Mater.*, 2018, **30**.

39. X. Li, C. Zhang, M. Luo, Q. Yao and Z.-H. Lu, *Inorg. Chem. Front.*, 2020, **7**, 1298-1306.

40. S. Y. Ding, J. Gao, Q. Wang, Y. Zhang, W. G. Song, C. Y. Su and W. Wang, *J. Am. Chem. Soc.*, 2011, **133**, 19816-19822.

41. P. Pachfule, M. K. Panda, S. Kandambeth, S. M. Shivaprasad and R. Banerjee, *J. Mater. Chem. A*, 2014, **2**, 7944-7952.

42. M. Bhadra, H. S. Sasmal, A. Basu, S. P. Midya, S. Kandambeth, P. Pachfule, E. Balaraman and R. Banerjee, *ACS Appl. Mater. Inter.*, 2017, **9**, 13785-13792.

43. Y. Deng, Z. Zhang, P. Du, X. Ning, Y. Wang, D. Zhang, J. Liu, S. Zhang and X. Lu, *Angew. Chem. Int. Ed.*, 2020, **59**, 6082-6089.

44. S. Liu and Y. J. Xu, *Sci. Rep.*, 2016, **6**, 22742.

45. M. Liu, X. Wang, J. Liu, K. Wang, S. Jin and B. Tan, *ACS Appl. Mater. Inter.*, 2020, **12**, 12774-12782.

46. Y. Xia, K. D. Gilroy, H. C. Peng and X. Xia, *Angew. Chem. Int. Ed.*, 2017, **56**, 60-95.

47. R. Luo, M. Chen, X. Liu, W. Xu, J. Li, B. Liu and Y. Fang, *J. Mater. Chem. A*, 2020, **8**, 18408-18424.

48. D. Wang, H. Zeng, X. Xiong, M.-F. Wu, M. Xia, M. Xie, J.-P. Zou and S.-L. Luo, *Sci. Bull.*, 2020, **65**, 113-122.

49. Y. Yao, H. Yin, M. Gao, Y. Hu, H. Hu, M. Yu and S. Wang, *Chem. Eng. Sci.*, 2019, **209**, 115211.

50. J. H. Li, Z. W. Yu, Z. Gao, J. Q. Li, Y. Tao, Y. X. Xiao, W. H. Yin, Y. L. Fan, C. Jiang, L. J. Sun and F. Luo, *Inorg. Chem.*, 2019, **58**, 10829-10836.

51. Q. Sun, B. Aguila, J. Perman, L. D. Earl, C. W. Abney, Y. Cheng, H. Wei, N. Nguyen, L. Wojtas and S. Ma, *J Am. Chem. Soc.*, 2017, **139**, 2786-2793.

52. C. E. Chan-Thaw, A. Villa, P. Katekomol, D. Su, A. Thomas and L. Prati, *Nano.*

View Article Online
DOI: 10.1039/D1TA04439G

Lett., 2010, **10**, 537-541.

53. M. Pilaski, J. Artz, H.-U. Islam, A. M. Beale and R. Palkovits, *Micropor. Mesopor. Mat.*, 2016, **227**, 219-227.

54. S. Ghosh, T. S. Khan, A. Ghosh, A. H. Chowdhury, M. A. Haider, A. Khan and S. M. Islam, *ACS Sustain. Chem. Eng.*, 2020, **8**, 5495-5513.

55. S. Qiu, Q. Fang, H. Li, X. Guan and Y. Yusran, *Natl. Sci. Rev.*, 2020, **7**, 170-190.

56. Y. Xiang, W. Dong, P. Wang, S. Wang, X. Ding, F. Ichihara, Z. Wang, Y. Wada, S. Jin, Y. Weng, H. Chen and J. Ye, *Appl. Catal. B*, 2020, **274**, 119096.

57. Y. Fu, X. Zhu, L. Huang, X. Zhang, F. Zhang and W. Zhu, *Appl. Catal. B*, 2018, **239**, 46-51.

58. J. Bi, B. Xu, L. Sun, H. Huang, S. Fang, L. Li and L. Wu, *ChemPlusChem*, 2019, **84**, 1149-1154.

59. Q.-P. Zhang, Y.-l. Sun, G. Cheng, Z. Wang, H. Ma, S.-Y. Ding, B. Tan, J.-h. Bu and C. Zhang, *Chem. Eng. J.*, 2020, **391**, 123471.

60. C. S. Diercks and O. M. Yaghi, *Science*, 2017, **355**.

61. X. Shi, Y. Yao, Y. Xu, K. Liu, G. Zhu, L. Chi and G. Lu, *ACS Appl. Mater. Inter.*, 2017, **9**, 7481-7488.

62. K. Cui, W. Zhong, L. Li, Z. Zhuang, L. Li, J. Bi and Y. Yu, *Small*, 2019, **15**, e1804419.

63. S. Nandi, S. K. Singh, D. Mullangi, R. Illathvalappil, L. George, C. P. Vinod, S. Kurungot and R. Vaidhyanathan, *Adv. Energy Mater.*, 2016, **6**, 13465–13473.

64. M. E. G. Feng Tao, Yawen Zhang, Derek R. Butcher, James R. Renzas, Zhi Liu, Jen Y. Chung, Bongjin S. Mun, Miquel Salmeron, Gabor A. Somorjai, *Science*, 2008, **322**, 932-934.

65. S. Lu, Y. Hu, S. Wan, R. McCaffrey, Y. Jin, H. Gu and W. Zhang, *J Am. Chem. Soc.*, 2017, **139**, 17082-17088.

66. J. Liu, H. Zhan, N. Wang, Y. Song, C. Wang, X. Wang, L. Ma and L. Chen, *ACS Appl. Nano Mater.*, 2021, **4**, 6239-6249.

67. D. Mullangi, D. Chakraborty, A. Pradeep, V. Koshti, C. P. Vinod, S. Panja, S. Nair and R. Vaidhyanathan, *Small*, 2018, **14**, e1801233.

68. N. Wang, J. Liu, L. Tang, X. Wei, C. Wang, X. Li and L. Ma, *ACS Appl. Mater. Inter.*, 2021, **13**, 24966-24975.

69. G. J. Chen, X. B. Li, C. C. Zhao, H. C. Ma, J. L. Kan, Y. B. Xin, C. X. Chen and Y. B. Dong, *Inorg. Chem.*, 2018, **57**, 2678-2685.

70. C. Xu, J. Lin, D. Yan, Z. Guo, D. J. Austin, H. Zhan, A. Kent and Y. Yue, *ACS Appl. Nano Mater.*, 2020, **3**, 6416-6422.

71. L. Ma, W. Hu, B. Mei, H. Liu, B. Yuan, J. Zang, T. Chen, L. Zou, Z. Zou, B. Yang, Y. Yu, J. Ma, Z. Jiang, K. Wen and H. Yang, *ACS Catal.*, 2020, **10**, 4534-4542.

72. C. Li, X. Ren, M. Guo, W. Li, H. Li and Q. Yang, *Catal. Sci. Technol.*, 2021, **11**, 3873-3879.

73. G. Wen, S. Pan, M. Gan, A. Liang and Z. Jiang, *ACS Appl. Bio Mater.*, 2021, **4**, 4582-4590.

74. E. Jin, Z. Lan, Q. Jiang, K. Geng, G. Li, X. Wang and D. Jiang, *Chem*, 2019, **5**, 1632-1647.

75. Y. Huang, P. Du, W.-X. Shi, Y. Wang, S. Yao, Z.-M. Zhang, T.-B. Lu and X. Lu, *Appl. Catal. B*, 2021, **288**, 120001

76. J. Li, P. Liu, Y. Tang, H. Huang, H. Cui, D. Mei and C. Zhong, *ACS Catal.*, 2020, **10**, 2431-2442.

77. K. Iwase, S. Nakanishi, M. Miyayama and K. Kamiya, *ACS Appl. Energy Mater.*, 2020, **3**, 1644-1652.

78. X. Wang, Z. Fu, L. Zheng, C. Zhao, X. Wang, S. Y. Chong, F. McBride, R. Raval, M. Bilton, L. Liu, X. Wu, L. Chen, R. S. Sprick and A. I. Cooper, *Chem. Mater.*, 2020, **32**, 9107-9114.

79. J. Wang, J. Wang, S. Qi and M. Zhao, *J. Phys. Chem. C*, 2020, **124**, 17675-17683.

80. F. Lu and D. Astruc, *Coord. Chem. Rev.*, 2018, **356**, 147-164.

81. Y. Wu, B. Dong, J. Zhang, H. Song and C. Yan, *Int. J. Hydrog. Energy*, 2018, **43**, 12627-12636.

82. Q.-L. Zhu and Q. Xu, *Chem*, 2016, **1**, 220-245.

83. K. Chen, L. Yang, Z. Wu, C. Chen, J. Jiang and G. Zhang, *Phys. Chem. Chem. Phys.*, 2019, **21**, 546-553.

84. J. Wang and S. Zhuang, *Coord. Chem. Rev.*, 2019, **400**, 213046.

85. S. Y. Ding and W. Wang, *Chem. Soc. Rev.*, 2013, **42**, 548-568.

86. J. L. Segura, M. J. Mancheno and F. Zamora, *Chem. Soc. Rev.*, 2016, **45**, 5635-

View Article Online
DOI: 10.1039/D1TA04439G

5671.

87. Y. Liu, Y. Yang, Y. Sun, J. Song, N. G. Rudawski, X. Chen and W. Tan, *J Am. Chem. Soc.*, 2019, **141**, 7407-7413.

88. W. C. Conner and J. L. Falconer, *Chem. Rev.*, 2002, **95**, 759-788.

89. S. Kato, K. Iwase, T. Harada, S. Nakanishi and K. Kamiya, *ACS App.l Mater. Inter.*, 2020, **12**, 29376-29382.

90. D. J. Xiao, E. D. Bloch, J. A. Mason, W. L. Queen, M. R. Hudson, N. Planas, J. Borycz, A. L. Dzubak, P. Verma, K. Lee, F. Bonino, V. Crocella, J. Yano, S. Bordiga, D. G. Truhlar, L. Gagliardi, C. M. Brown and J. R. Long, *Nat. chem.*, 2014, **6**, 590-595.

91. H.-C. Ma, J.-L. Kan, G.-J. Chen, C.-X. Chen and Y.-B. Dong, *Chem. Mater.*, 2017, **29**, 6518-6524.

92. P. Z. Li, X. J. Wang, J. Liu, J. S. Lim, R. Zou and Y. Zhao, *J. Am. Chem. Soc.*, 2016, **138**, 2142-2145.

93. J. Ming, A. Liu, J. Zhao, P. Zhang, H. Huang, H. Lin, Z. Xu, X. Zhang, X. Wang, J. Hofkens, M. B. J. Roeffaers and J. Long, *Angew. Chem. Int. Ed.*, 2019, **58**, 18290-18294.

94. S. Wang, X. Hai, X. Ding, S. Jin, Y. Xiang, P. Wang, B. Jiang, F. Ichihara, M. Oshikiri, X. Meng, Y. Li, W. Matsuda, J. Ma, S. Seki, X. Wang, H. Huang, Y. Wada, H. Chen and J. Ye, *Nat. Commun.*, 2020, **11**, 1149.

95. A. Mukhtar, S. Saqib, N. B. Mellon, S. Rafiq, M. Babar, S. Ullah, N. Muhammad, A. L. Khan, M. Ayoub, M. Ibrahim, K. Maqsood, M. A. Bustam,

A. G. Al-Sehemi, J. J. Klemeš, S. Asif and A. Bokhari, *J. Clean. Prod.*, 2020, **277**, 123999.

96. E. Park, J. Jack, Y. Hu, S. Wan, S. Huang, Y. Jin, P. C. Maness, S. Yazdi, Z. Ren and W. Zhang, *Nanoscale*, 2020, **12**, 2596-2602.

97. B. J. Murray, T. W. Wilson, S. Dobbie, Z. Cui, S. M. R. K. Al-Jumur, O. Möhler, M. Schnaiter, R. Wagner, S. Benz, M. Niemand, H. Saathoff, V. Ebert, S. Wagner and B. Kärcher, *Nat. Geosci.*, 2010, **3**, 233-237.

98. K. Cui, W. Zhong, L. Li, Z. Zhuang, L. Li, J. Bi and Y. Yu, *Small*, 2018, **15**, 1804419.

99. M. Bhadra, S. Kandambeth, M. K. Sahoo, M. Addicoat, E. Balaraman and R. Banerjee, *J Am. Chem. Soc.*, 2019, **141**, 6152-6156.

100. D. Chakraborty, S. Nandi, D. Mullangi, S. Haldar, C. P. Vinod and R. Vaidhyanathan, *ACS Appl. Mater. Inter.*, 2019, **11**, 15670-15679.

101. M. Zhang, Y. Li, W. Yuan, X. Guo, C. Bai, Y. Zou, H. Long, Y. Qi, S. Li, G. Tao, C. Xia and L. Ma, *Angew. Chem. Int. Ed.*, 2021, **60**, 12396-12405.

102. J. Thote, H. B. Aiyappa, A. Deshpande, D. Diaz Diaz, S. Kurungot and R. Banerjee, *Chem. Eur. J.*, 2014, **20**, 15961-15965.

103. C. Z. Xiugang Li, Minghong Luo, Qilu Yao, Zhang-Hui Lu, *Inorg. Chem. Front.*, 2020, **7**, 1298-1306.

104. J.-L. K. Hui-Chao Ma, Gong-Jun Chen, Cheng-Xia Chen, and Yu-Bin Dong, *Chem. Mater.*, 2017, **29**, 6518-6524.

105. M. B. Ross, J. C. Ku, V. M. Vaccarezza, G. C. Schatz and C. A. Mirkin, *Nat.*

View Article Online
DOI: 10.1039/D1TA04439G

Nanotechnol., 2015, **10**, 453-458.

106. M. Liu, W. Xu, J. Bai, C. K. Chua, J. Wei, Z. Li, Y. Gao, D. H. Kim and K. Zhou, *Nanotechnology*, 2016, **27**, 405703.

107. J. Zhang, X. Han, X. Wu, Y. Liu and Y. Cui, *J. Am. Chem. Soc.*, 2017, **139**, 8277-8285.

108. P. Kour and S. P. Mukherjee, *J. Mater. Chem. A*, 2021, **9**, 6819-6826.

109. H. Konnerth, B. M. Matsagar, S. S. Chen, M. H. G. Prechtl, F.-K. Shieh and K. C. W. Wu, *Coord. Chem. Rev.*, 2020, **416**, 213319.

110. R. Qin, P. Liu, G. Fu and N. Zheng, *Small Methods*, 2018, **2**, 1700286.

111. H. Ma, H. Ren, S. Meng, F. Sun and G. Zhu, *Sci. Rep.*, 2013, **3**, 2611.

112. J. K. Nørskov, T. Bligaard, A. Logadottir, S. Bahn, L. B. Hansen, M. Bollinger, H. Bengaard, B. Hammer, Z. Sljivancanin, M. Mavrikakis, Y. Xu, S. Dahl and C. J. H. Jacobsen, *J. Catal.*, 2002, **209**, 275-278.

113. J. M. Thomas, *Nat. Catal.*, 2018, **1**, 2-5.

114. L. Liu, D. M. Meira, R. Arenal, P. Concepcion, A. V. Puga and A. Corma, *ACS Catal.*, 2019, **9**, 10626-10639.

115. C. L. Yao, J. C. Li, W. Gao and Q. Jiang, *Chemistry*, 2018, **24**, 11051-11058.

116. K. Guo, X. Zhu, L. Peng, Y. Fu, R. Ma, X. Lu, F. Zhang, W. Zhu and M. Fan, *Chem. Eng. J.*, 2021, **405**, 127011.

117. F. Pan, F. Xiao and N. Wang, *Appl. Surf. Sci.*, 2021, **565**, 107-114.

118. J. Wang, Z. Zhang, S. Qi, Y. Fan, Y. Yang, W. Li and M. Zhao, *J. Mater. Chem. A*, 2021.

View Article Online
DOI: 10.1039/D1TA04439G

119. H. K. Fujishima A, *Nature*, 1972, **238**, 37-38.

120. Y. Ding, I. S. Yang, Z. Li, X. Xia, W. I. Lee, S. Dai, D. W. Bahnemann and J. H. Pan, *Prog. Mater. Sci.*, 2020, **109**, 100620.

121. J. Liu, Y. Wang, J. Ma, Y. Peng and A. Wang, *J. Alloys Compd.*, 2019, **783**, 898-918.

122. L. Cheng, Q. Xiang, Y. Liao and H. Zhang, *Energy Environ. Sci.*, 2018, **11**, 1362-1391.

123. L. Li, J. J. Wang, Y. Zhao, B. Ding, X. G. Wang, X. J. Zhao and E. C. Yang, *Nanotechnology*, 2021, **32**, 045710.

124. X. Li, J. Xiong, X. Gao, J. Huang, Z. Feng, Z. Chen and Y. Zhu, *J. Alloys Compd.*, 2019, **802**, 196-209.

125. B. P. Biswal, H. A. Vignolo-Gonzalez, T. Banerjee, L. Grunenberg, G. Savasci, K. Gottschling, J. Nuss, C. Ochsenfeld and B. V. Lotsch, *J. Am. Chem. Soc.*, 2019, **141**, 11082-11092.

126. T. Banerjee, K. Gottschling, G. Savasci, C. Ochsenfeld and B. V. Lotsch, *ACS Energy Lett.*, 2018, **3**, 400-409.

127. K. Gottschling, G. Savasci, H. Vignolo-Gonzalez, S. Schmidt, P. Mauker, T. Banerjee, P. Rovo, C. Ochsenfeld and B. V. Lotsch, *J. Am. Chem. Soc.*, 2020, **142**, 12146-12156.

128. A. W. Achtstein, O. Marquardt, R. Scott, M. Ibrahim, T. Riedl, A. V. Prudnikau, A. Antanovich, N. Owschimikow, J. K. N. Lindner, M. Artemyev and U. Woggon, *ACS Nano.*, 2018, **12**, 9476-9483.

View Article Online
DOI: 10.1039/D1TA04439G

129. C. Cheng, B. He, J. Fan, B. Cheng, S. Cao and J. Yu, *Adv. Mater.*, 2021, **33**, e2100317.

130. C. Zhou, S. Wang, Z. Zhao, Z. Shi, S. Yan and Z. Zou, *Adv. Funct. Mater.*, 2018, **28**, 1801214.

131. P. Yating, Q. Yunyang, Z. Xusheng, C. Sheng-Qi, Y. Yijun, D. Chunmei, W. Xi, Y. Shu-Hong and J. Hai-Long, *Natl. Sci. Rev.*, 2021, **42**, 107-114.

132. L. R. MacFarlane, H. Shaikh, J. D. Garcia-Hernandez, M. Vespa, T. Fukui and I. Manners, *Nat. Rev. Mater.*, 2020, **6**, 7–26.

133. Y.-H. Lee, Y.-P. Lee, C.-J. Chiang, C. Shen, Y.-H. Chen, L. Wang and C.-A. Dai, *Macromolecules*, 2014, **47**, 5551-5557.

134. A. C. Deacy, A. F. R. Kilpatrick, A. Regoutz and C. K. Williams, *Na.t Chem.*, 2020, **12**, 372-380.

135. T. K. Pal, D. De and P. K. Bharadwaj, *Coord. Chem. Rev.*, 2020, **408**, 213173.

136. Y. Ma, Z. Wang, X. Xu and J. Wang, *Chinese J. Catal.*, 2017, **38**, 1956-1969.

137. T. Kong, Y. Jiang and Y. Xiong, *Chem. Soc. Rev.*, 2020, **49**, 6579-6591.

138. Z. Jiang, X. Xu, Y. Ma, H. S. Cho, D. Ding, C. Wang, J. Wu, P. Oleynikov, M. Jia, J. Cheng, Y. Zhou, O. Terasaki, T. Peng, L. Zan and H. Deng, *Nature*, 2020, **586**, 549-554.

139. Y. Wang, X. Liu, X. Han, R. Godin, J. Chen, W. Zhou, C. Jiang, J. F. Thompson, K. B. Mustafa, S. A. Shevlin, J. R. Durrant, Z. Guo and J. Tang, *Nat. Commun.*, 2020, **11**, 2531.

140. D.-G. Wang, T. Qiu, W. Guo, Z. Liang, H. Tabassum, D. Xia and R. Zou,

View Article Online
DOI: 10.1039/D1TA04439G

Energy Environ. Sci., 2020, **14**, 688-728.

141. W. Zhong, R. Sa, L. Li, Y. He, L. Li, J. Bi, Z. Zhuang, Y. Yu and Z. Zou, *J. Am. Chem. Soc.*, 2019, **141**, 7615-7621.

142. R. K. Yadav, A. Kumar, N.-J. Park, K.-J. Kong and J.-O. Baeg, *J. Mater. Chem. A*, 2016, **4**, 9413-9418.

143. C. Dong, Y. Li, D. Cheng, M. Zhang, J. Liu, Y.-G. Wang, D. Xiao and D. Ma, *ACS Catal.*, 2020, **10**, 11011-11045.

144. N. Huang, P. Wang and D. Jiang, *Nat. Rev. Mater.*, 2016, **1**, 16068.

145. K. Y. Foo and B. H. Hameed, *Adv. Colloid Interface Sci.*, 2010, **159**, 130-143.

146. Y. Qin, H. Li, J. Lu, F. Meng, C. Ma, Y. Yan and M. Meng, *Chem. Eng. J.*, 2020, **384**, 123275.

147. W. Jiang, D. Qu, L. An, X. Gao, Y. Wen, X. Wang and Z. Sun, *J. Mater. Chem. A*, 2019, **7**, 18348-18356.

148. X. Zhu, Y. Lin, J. San Martin, Y. Sun, D. Zhu and Y. Yan, *Nat. Commun.*, 2019, **10**, 2843.

149. T. Li, C. Atish, K. Silambarasan, X. Liu and A. P. O'Mullane, *Electrochim. Acta*, 2020, **362**, 137212.

150. C. Bae, T. A. Ho, H. Kim, S. Lee, S. Lim, M. Kim, H. Yoo, J. M. Montero-Moreno, J. H. Park and H. Shin, *Sci. Adv.*, 2017, **3**, e1602215.

151. S. Dey, B. Mondal, S. Chatterjee, A. Rana, S. Amanullah and A. Dey, *Nat. Rev. Chem.*, 2017, **1**, 1-20.

152. A. P. Dam, G. Papakonstantinou and K. Sundmacher, *Sci. Rep.*, 2020, **10**, 14140.

View Article Online
DOI: 10.1039/D1TA04439G

153. L. Fan, C. Xia, F. Yang, J. Wang and Y. Lu, *Sci. Adv.*, 2020, **6**, eaay3111.

154. D. H. Kweon, M. S. Okyay, S. J. Kim, J. P. Jeon, H. J. Noh, N. Park, J. Mahmood and J. B. Baek, *Nat. commun.*, 2020, **11**, 1278.

155. Y. Y. Birdja, E. Pérez-Gallent, M. C. Figueiredo, A. J. Göttle, F. Calle-Vallejo and M. T. M. Koper, *Nat. Energy*, 2019, **4**, 732-745.

156. Y. Wang, J. Liu, Y. Wang, Y. Wang and G. Zheng, *Nat. Commun.*, 2018, **9**, 5003.

157. S. Lin, C. S. Diercks, Y. B. Zhang, N. Kornienko, E. M. Nichols, Y. Zhao, A. R. Paris, D. Kim, P. Yang, O. M. Yaghi and C. J. Chang, *Science*, 2015, **349**, 1208-1213.

158. J. Huang, N. Hormann, E. Oveisi, A. Loiudice, G. L. De Gregorio, O. Andreussi, N. Marzari and R. Buonsanti, *Nat. commun.*, 2018, **9**, 3117.

159. M. Zhou, H. L. Wang and S. Guo, *Chem. Soc. Rev.*, 2016, **45**, 1273-1307.

160. X. Han, K. Wang, G. Zhang, W. Gao and J. Chen, *Adv, Synth. Catal.*, 2019, **361**, 2804-2824.

161. P. Liu, J. Ran, B. Xia, S. Xi, D. Gao and J. Wang, *Nano-Micro Lett.*, 2020, **12**, 68.

162. L. Chen, X. Xu, W. Yang and J. Jia, *Chinese Chem. Lett.*, 2020, **31**, 626-634.

163. R. Ma, G. Lin, Y. Zhou, Q. Liu, T. Zhang, G. Shan, M. Yang and J. Wang, *NPJ Comput. Mater.*, 2019, **5**, 78.

164. Z. Li, H. Zhang, L. Wang, X. Meng, J. Shi, C. Qi, Z. Zhang, L. Feng and C. Li, *J. Photochem. Photobiol. A*, 2020, **386**, 112099.

View Article Online
DOI: 10.1039/D1TA04439G

165. Y. Liu, H. Xu, H. Yu, H. Yang and T. Chen, *Sci. Rep.*, 2020, **10**, 20075.

166. K. Kuroda, T. Ishida and M. Haruta, *J. Mol. Cata.l A Chem.*, 2009, **298**, 7-11.

167. M. H. a and M. D. b, *Appl. Catal. A-Gen.*, 2001, **222**, 427-437.

168. S. Gu, Y. Lu, J. Kaiser, M. Albrecht and M. Ballauff, *Phys. Chem. Chem. Phy.s*, 2015, **17**, 28137-28143.

169. M. Schrinner, F. Polzer, Y. Mei, Y. Lu, B. Haupt, M. Ballauff, A. Göldel, M. Drechsler, J. Preussner and U. Glatzel, *Macromol Chem. Phys.*, 2007, **208**, 1542-1547.

170. J. A. R. Navarro, *Science*, 2018, **361**, 35.

171. Y. Song, Z. Li, P. Ji, M. Kaufmann, X. Feng, J. S. Chen, C. Wang and W. Lin, *ACS Catal.*, 2019, **9**, 1578-1583.

172. A. M. Abdalla, S. Hossain, O. B. Nisfindy, A. T. Azad, M. Dawood and A. K. Azad, *Energy Convers. Manag.*, 2018, **165**, 602-627.

173. F. R. Fortea-Perez, M. Mon, J. Ferrando-Soria, M. Boronat, A. Leyva-Perez, A. Corma, J. M. Herrera, D. Osadchii, J. Gascon, D. Armentano and E. Pardo, *Nat. Mater.*, 2017, **16**, 760-766.

174. G. Li, S. Zhao, Y. Zhang, and Z. Tang, *Adv. Mater.*, 2018, **30**, 1800702.

175. C. Li, C. Paris, J. Martínez-Triguero, M. Boronat, M. Moliner and A. Corma, *Nat. Catal.*, 2018, **1**, 547-554.